AIMS Mathematics, 10(3): 5021–5051.
DOI: 10.3934/math.2025230
Received: 23 October 2024
Revised: 08 January 2025
Accepted: 13 February 2025
Published: 06 March 2025

https://www.aimspress.com/journal/Math

Research article

Exploring three periodic point dynamics in 2D spatiotemporal discrete systems

Mohamed Lamine Sahari[1,*], **Abdel-Kaddous Taha**[2,*] **and Louis Randriamihamison**[3,*]

[1] LANOS Laboratory, Department of Mathematics, Badji Mokhtar-Annaba University, P. O. Box 12, 23000 Annaba, Algeria

[2] INSA, Federal University of Toulouse Midi-Pyrénées, 135 Avenue de Rangueil, 31077 Toulouse Cedex 4, France

[3] IPST-Cnam, Institut National Polytechnique de Toulouse, University of Toulouse, 118, route de Narbonne, 31062 Toulouse Cedex 9, France

* **Correspondence:** Email: mohamed-lamine.sahari@univ-annaba.dz, taha@insa-toulouse.fr, louis.randriamihamison@ipst.fr.

Abstract: This paper explores the dynamics of 2D spatiotemporal discrete systems, focusing on the stability and bifurcations of periodic solutions, particularly 3-cycles. After introducing the concept of a third-order cycle, we discuss both numerical and analytical techniques used to analyze these cycles, defining four types of 3-periodic points and their associated stability conditions. As a specific case, this study examines a spatiotemporal quadratic map, analyzing the existence of 3-cycles and various bifurcation scenarios, such as fold and flip bifurcations, as well as chaotic behavior. In 2D spatiotemporal systems, quadratic maps intrinsically offer better conditions that favor the emergence of chaos, which is characterized by high sensitivity to initial conditions. The findings emphasize the complexity of these systems and the crucial role of bifurcation curves in understanding stability regions. The paper concludes with key insights and suggestions for future research in this field.

Keywords: Chaos; bifurcation; bifurcation curves; 2D spatiotemporal discrete systems; spectrum; stability
Mathematics Subject Classification: 47A10, 37G10, 37G35, 37L15

1. Introduction

Understanding the dynamics of complex systems is fundamental for grasping a wide array of natural phenomena, from chemical reactions to population dynamics [1–5]. Over the past few decades, significant attention has been devoted to the study of spatiotemporal systems, where both

spatial and temporal dimensions interact to shape system behavior [6–9]. In particular, two-dimensional (2D) spatiotemporal discrete systems have attracted considerable interest for their applications in various fields, such as digital filtering, image processing, encryption, spatial dynamical systems, and numerical solutions for partial differential equations [10–19].

Analyzing the dynamics of periodic points in spatiotemporal discrete systems is critical for identifying complex behaviors, such as stability transitions, bifurcations, and chaos. These phenomena are not only of theoretical interest, but also have significant implications across various fields. For example, in ecology, periodic cycles are essential in modeling predator-prey interactions, where stability transitions can predict population oscillations [4, 20]. In engineering, such dynamics inform the design of synchronized networks critical for secure communications and reliable systems [5]. Similarly, in physics, wave propagation in discrete media, such as electrical networks and mechanical systems, relies on understanding spatiotemporal patterns and transitions [1]. Our results also intersect with neuroscience, where models like the Nagumo-FitzHugh equations describe neural excitations and transitions to complex states [21].

This work aims to contribute to these fields by establishing a rigorous mathematical framework for analyzing 3-periodic point dynamics and their bifurcations, providing valuable tools for predicting and understanding intricate behaviors in spatiotemporal systems. Building on this extensive body of research, this paper focuses on the stability and bifurcations in 2D spatiotemporal discrete systems, with a particular emphasis on periodic solutions of period three. We employ analytical and numerical techniques to examine the stability of these 3-cycles, and investigate a range of bifurcation scenarios. This work extends the analysis presented in our earlier publication [22], continuing the exploration of bifurcations in 2D spatiotemporal maps [23, 24], and providing deeper insights into the complexity of such systems.

We are particularly interested in studying the 2D spatiotemporal discrete system

$$x_{m+1,n+1} = f(x_{m,n}, x_{m+1,n}), \tag{1.1}$$

where $m \in \mathbb{Z}$ and $n \in \mathbb{N}$ represent the spatial coordinate and the time, respectively. The function $f : \mathbb{R}^2 \longrightarrow \mathbb{R}$ is a nonlinear function with bounded variation.

From (1.1), we can define a 1-D recurrence on the space

$$X := \left\{ [x] := (x_i)_{i=-\infty}^{\infty} \in \mathbb{R}^{\mathbb{Z}} : \|[x]\| = \sqrt{\sum_{i=-\infty}^{\infty} q^{-|i|} x_i^2} < \infty,\ q > 0 \right\},$$

as follows: For an initial condition $[x]_0 = (x_{m,0})_{m=-\infty}^{\infty} \in X$, called the "boundary condition", we recursively construct a sequence of solutions

$$\left\{ [x]_n = (x_{m,n})_{m=-\infty}^{\infty},\ n = 0, 1, 2, \ldots \right\} \subset X,$$

by

$$[x]_{n+1} = \left(f(x_{m-1,n}, x_{m,n}) \right)_{m=-\infty}^{\infty}. \tag{1.2}$$

Alternatively, if $F : X \longrightarrow X$ is the map defined by

$$F([x]) = (f(x_{i-1}, x_i))_{i=-\infty}^{\infty}, \tag{1.3}$$

for all $[x] = (x_i)_{i=-\infty}^{i=\infty} \in X$, then system (1.1) is equivalent to the following infinite-dimensional discrete dynamical system:

$$[x]_{n+1} = F([x]_n). \tag{1.4}$$

The map F defined by (1.3)-(1.4) is said to be induced by system (1.1). Clearly, a sequence $\{[x]_n, n = 0, 1, 2, \ldots\}$ is a solution of system (1.1) if and only if it is a solution of system (1.4) (see [23, 24]).

In our previous work [23, 24], we defined various forms of cycles for $k = 1$ and $k = 2$, and provided the necessary and sufficient conditions for their stability. In the present study, we define four types of 3rd-order cycles and present the necessary and sufficient conditions for determining their stability.

The rest of the paper is structured as follows:

In Section 2, we analyze the properties of nonlinear dynamics, singularities, and basic bifurcations in two-dimensional spatiotemporal discrete systems. Definitions 1 and 2 introduce the concept of a cycle of order k. In Section 2.1, we defined the four types of 3-periodic points considered in this study. Theorem 1 presents the main result on the stability of these cycles.

In Section 3, we investigate a spatiotemporal quadratic map. In Section 3.1, we review the results on cycles for $k = 1$ and $k = 2$, as well as their corresponding bifurcations. Theorems 3, 4, and 5 present these findings, while Figure 7 provides visual illustrations of the complexity of the nonlinear problem under investigation. Section 3.2 focuses on the existence of 3-cycles in the spatiotemporal quadratic map. The definitions and propositions in this section introduce the analytical expressions for the four types of third-order cycles considered in this study. In Section 3.4, we explore bifurcations in a spatiotemporal quadratic map based on the parameters (a, b). This study examines bifurcation curves, such as fold and flip bifurcations, for various cycles. These curves define regions of stability, semi-stability, and instability within the parameter plane. The analysis highlights singular points where bifurcation curves intersect or become tangent, illustrating the emergence and modification of stability regions.

Finally, in Section 4 we draw relevant conclusions and discuss future perspectives for our research in this context.

2. Singularities and basic bifurcations in 2D spatiotemporal discrete systems

Consider the function $f^{[k]} : \mathbb{R}^{k+1} \longrightarrow \mathbb{R}$, defined recursively as follows:

$$\begin{cases} f^{[1]}(x_0, x_1) := f(x_0, x_1), \\ f^{[2]}(x_0, x_1, x_2) := f\left(f(x_0, x_1), f(x_1, x_2)\right), \\ f^{[k]}(x_0, \ldots, x_k) := f\left(f^{[k-1]}(x_0, \ldots, x_{k-1}), f^{[k-1]}(x_1, \ldots, x_k)\right), \quad (x_0, \ldots, x_k) \in \mathbb{R}^{k+1}. \end{cases}$$

Definition 1. *For $k \in \mathbb{N}^*$, the map $F^k : X \to X$ is defined as*

1. $F^0([x]) := I([x]) = [x]$,
2. $F^k([x]) := F\left(F^{k-1}([x])\right)$ *for all* $[x] \in X$.

Definition 2. *A sequence $P_k = \left(x_i^*\right)_{i=-\infty}^{\infty} \in X$ is called a periodic point of period k (or a k-cycle, k-periodic point) for the dynamical system (1.1) if*

1. $F^k(P_k) = P_k$, *i.e.*, $f^{[k]}(x^*_{j-k}, \ldots, x^*_j) = x^*_j$ *for all* $j \in \mathbb{Z}$,
2. $F^r(P_k) \neq P_k$ *for all* $r < k$. *That is, for every* $r < k$, *there exists at least one integer* j *such that*

$$f^{[r]}(x^*_{j-r}, \ldots, x^*_j) \neq x^*_j.$$

The set $\left\{P_k, F(P_k), \ldots, F^{k-1}(P_k)\right\}$ *is called a k-periodic orbit.*

Remark 1. *Due to the complexity of the calculations, we often focus on specific types of singularities, detailed as follows:*

1. *The k-cycle of the form* $(x_{i \mod j})_{i=-\infty}^{\infty}$, *where* $j \in \mathbb{N}$, *is denoted by* k_j.
2. *A 1-periodic point (also known as a fixed point or 1-cycle)* $P_1 = \left(x^*_i\right)_{i=-\infty}^{\infty}$ *is of type* 1_1 *if* $x^*_i = x^* \in \mathbb{R}$ *for all* $i \in \mathbb{Z}$, *and of type* 1_2 *if there exist two real numbers* x^* *and* y^* *such that* $x^*_{2i} = x^*$ *and* $x^*_{2i+1} = y^*$ *for all* $i \in \mathbb{Z}$.
   Similarly, we can define a 1-periodic point of type 1_n *for* $n \in \mathbb{N}^*$.
3. *A 2-periodic point (also called a 2-cycle)* $P_2 = \left(x^*_i\right)_{i=-\infty}^{\infty}$ *is of horizontal type (H) or type* 2_1 *if* $x^*_i = x^* \in \mathbb{R}$ *for all* $i \in \mathbb{Z}$, *and of diagonal type (D) or* 2_2 *if there exist two real numbers* x^* *and* y^* *such that* $x^*_{2i} = x^*$ *and* $x^*_{2i+1} = y^*$, $f(x^*, y^*) = x^*$, *and* $f(y^*, x^*) = y^*$ *for all* $i \in \mathbb{Z}$.
   In our study, a 2-periodic point $P_2 = \left(x^*_i\right)_{i=-\infty}^{\infty}$ *is considered general if there exist two real numbers* x^* *and* y^* *such that* $x^*_{2i} = x^*$ *and* $x^*_{2i+1} = y^*$, *and* $[x]^*$ *is of neither type* 2_1 *nor* 2_2.

2.1. Types of 3-periodic points

A 3-periodic point (also called a 3-cycle) $P_3 = \left(x^*_i\right)_{i=-\infty}^{\infty}$ can be classified into four types:

1. **Horizontal type (H) or 3_1 type**: This occurs when $x^*_i = x^* \in \mathbb{R}$ for all $i \in \mathbb{Z}$. In this case, there exist three real numbers x^*, y^*, and z^* such that $x^* \neq f(x^*, x^*) = y^*$, $y^* \neq f(y^*, y^*) = z^*$, and $z^* \neq f(z^*, z^*) = x^*$ for all $i \in \mathbb{Z}$ (see Figure 1).
2. **Diagonal type (D) or 3_{3+} type:** This occurs when there exist three real numbers x^*, y^*, and z^* such that $z^* = x^*_{3i+2} \neq x^*_{3i} = x^* \neq y^* = x^*_{3i+1} \neq z^*$ and $f(x^*, y^*) = x^*$, $f(y^*, z^*) = y^*$, $f(z^*, x^*) = z^*$ for all $i \in \mathbb{Z}$ (see Figure 2).
3. **Super diagonal type (SD) or 3_2 type:** This occurs when there exist six real numbers x^*, y^*, z^*, t^*, u^*, v^* such that $z^* = f(y^*, x^*) \neq x^*_{3i} = x^* \neq y^* = x^*_{3i+1} \neq t^* = f(x^*, y^*) \neq z^*$, $u^* = f(t^*, z^*) \neq f(z^*, t^*) = v^*$, $f(v^*, u^*) = x^*$, and $f(u^*, v^*) = y^*$ for all $i \in \mathbb{Z}$ (see Figure 3).
4. **Anti diagonal type (AD) or 3_{3-} type:** If there exist three real numbers x^*, y^*, and z^* such that $z^* = x^*_{3i+2} \neq x^*_{3i} = x^* \neq y^* = x^*_{3i+1} \neq z^*$ and $f(x^*, y^*) = z^*$, $f(y^*, z^*) = x^*$, $f(z^*, x^*) = y^*$ for all $i \in \mathbb{Z}$ (see Figure 4).

Remark 2. *A 3-periodic point* $P_3 = \left(x^*_i\right)_{i=-\infty}^{\infty}$ *is said to be general if there exist three real numbers* x^*, y^*, *and* z^* *where* $z^* = x^*_{3i+2} \neq x^*_{3i} = x^* \neq y^* = x^*_{3i+1} \neq z^*$ *and* P_3 *is not type* 3_1, *not type* 3_2, *and not type* 3_3 *(see Figure 5).*

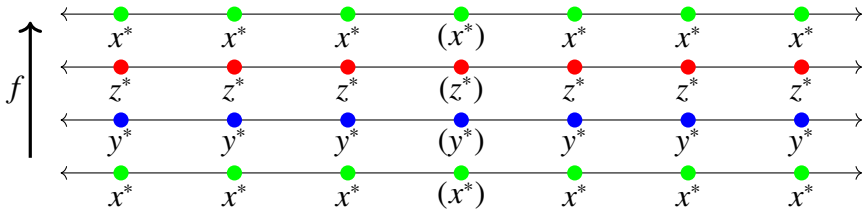

Figure 1. 3-periodic point of type H or 3_1 for f.

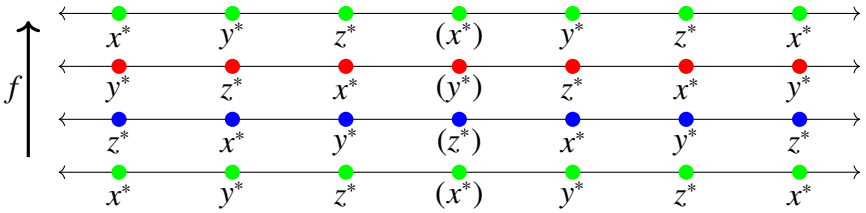

Figure 2. 3-periodic point of type D or 3_{3+} for f.

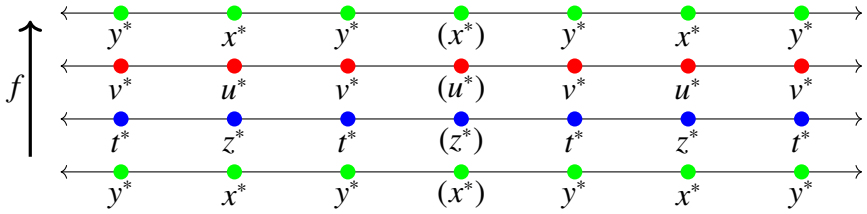

Figure 3. 3-periodic point of type SD or 3_2 for f.

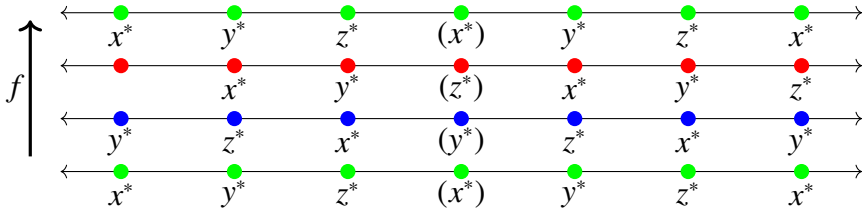

Figure 4. 3-periodic point of type AD or 3_{3-} for f.

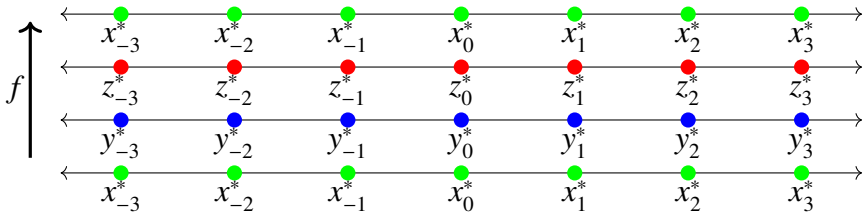

Figure 5. Genral 3-periodic point for f.

2.2. *Stability analysis*

Next, we present the conditions for the local stability of the recurrence relation (1.1) at a k-cycle point based on the results established in [23, 24].

Definition 3. *A k-cycle P_k of (1.1) is defined as:*

(1) *Stable if for every $\varepsilon > 0$ and $M \geq 0$ there exists $\delta > 0$ such that $\|[x] - P_k\| < \delta$ implies $\|F^m([x]) - P_k\| < \varepsilon$ for all $m \geq M$.*

(2) *Attracting (sink) if there exists $\delta > 0$ such that $\|[x] - P_k\| < \delta$ implies $\lim_{m\to+\infty} \|F^m([x]) - P_k\| = 0$.*

(3) *Repulsive if there exists $\delta > 0$ such that $\|[x] - P_k\| < \delta$ implies $\lim_{m\to-\infty} \|F^m([x]) - P_k\| = 0$.*

(4) *Asymptotically stable if it is both stable and attracting.*

(5) *Unstable if it is not stable.*

Remark 3. *A k-cycle P_k of map (1.1) is said to be semi-stable if it is unstable, and for every $\varepsilon > 0$ and $M \geq 0$ there exists $[x] \in X$ such that $\|F^m([x]) - P_k\| < \varepsilon$ for all $m \geq M$.*

The stability of a k-cycle P_k is determined by analyzing the spectrum $\sigma(J_{P_k})$ of the Jacobian matrix J_{P_k} at the k-cycle P_k. The matrix representing the Jacobian operator of the map F^k at a k-periodic point $P_k = (x^*_i)_{i=-\infty}^{\infty}$ is given by

$$J_{P_k} = \left[J_{i,j}\right]_{i,j\in\mathbb{Z}},$$

where

$$J_{i,j} = \begin{cases} \left(f^{[k]}_{x_{k+j-i}}\right)'(x^*_{j-k},\ldots,x^*_j) := \left.\dfrac{\partial f^{[k]}(x_0,\ldots,x_k)}{\partial x_{k+j-i}}\right|_{(x^*_{j-k},\ldots,x^*_j)} & \text{if } i-k \leq j \leq i, \\ 0 & \text{otherwise.} \end{cases}$$

We then have the following result:

Theorem 1. *Let $P_k \in X$ be a k-periodic point of (1.1), and let J_{P_k} be the Jacobian matrix of the map F^k at P_k. Then:*

(i) *If*

$$\sup\{|\lambda| : \lambda \in \sigma(J_{P_k})\} < 1,$$

then P_k is asymptotically stable.

(ii) *If*

$$\sup\{|\lambda| : \lambda \in \sigma(J_{P_k})\} > 1,$$

then P_k is unstable. Moreover, if

$$\inf\{|\lambda| : \lambda \in \sigma(J_{P_k})\} < 1,$$

then P_k is semi-stable.

(iii) *If*

$$\inf\{|\lambda| : \lambda \in \sigma(J_{P_k})\} > 1,$$

then P_k is repulsive.

Proof. The proof can be easily derived from [23, Proposition 1, p. 4] by using the fact that every k-periodic point of the map F is a fixed point for F^k . □

Determining the stability of k-cycles through the spectrum of the Jacobian matrix is a significant mathematical challenge (see [23–25]). Next, we present a stability result for the 3-cycle of type 3_1, where the spectrum of the Jacobian matrix has been well characterized. Consider the function $h : \mathbb{R}^4 \longrightarrow \mathbb{R}$ defined by $h := f^{[3]}$, where

$$h(x, y, z, t) = f(f(f(x, y), f(y, z)), f(f(y, z), f(z, t))).$$

The Jacobian matrix J_{P_3} of F^3 at the 3-cycle $P_3 = (x_i^*)_{i=-\infty}^{\infty} \in X$ is given by

$$J_{P_3} = \begin{pmatrix}
\ddots & \vdots & \vdots & \vdots & \vdots & \vdots & \ddots \\
\ddots & 0 & \vdots & \vdots & \vdots & \vdots & \ddots \\
\ddots & \Phi_{-2} & 0 & \vdots & \vdots & \vdots & \ddots \\
\ddots & \Psi_{-2} & \Phi_{-1} & 0 & \vdots & \vdots & \ddots \\
\ddots & \Omega_{-2} & \Psi_{-1} & [\Phi_0] & 0 & \vdots & \ddots \\
\ddots & \Theta_{-2} & \Omega_{-1} & \Psi_0 & \Phi_1 & 0 & \ddots \\
\ddots & 0 & \Theta_{-1} & \Omega_0 & \Psi_1 & \Phi_2 & \ddots \\
\ddots & \vdots & 0 & \Theta_0 & \Omega_1 & \Psi_2 & \ddots \\
\ddots & \vdots & \vdots & 0 & \Theta_1 & \Omega_2 & \ddots \\
\ddots & \vdots & \vdots & \vdots & 0 & \Theta_2 & \ddots \\
\ddots & \vdots & \vdots & \vdots & \vdots & 0 & \ddots \\
\ddots & \vdots & \vdots & \vdots & \vdots & \vdots & \ddots
\end{pmatrix}, \tag{2.1}$$

where

$$\begin{aligned}
\Phi_i &= h'_t(x^*_{i-3}, x^*_{i-2}, x^*_{i-1}, x^*_i), \\
\Psi_i &= h'_z(x^*_{i-2}, x^*_{i-1}, x^*_i, x^*_{i+1}), \\
\Omega_i &= h'_y(x^*_{i-1}, x^*_i, x^*_{i+1}, x^*_{i+2}), \\
\Theta_i &= h'_x(x^*_i, x^*_{i+1}, x^*_{i+2}, x^*_{i+3}).
\end{aligned} \tag{2.2}$$

The brackets around Φ_0 represent the 0-0 component of the matrix J_{P_3}.

Theorem 2. *Let $P_{3_1} = (x_i^* = x_{3_1}^*)_{i=-\infty}^{\infty}$ be a 3-periodic point of type 3_1 for system (3.1). Then, the spectrum of the Jacobian matrix $J_{P_{3_1}}$ is given by*

$$\sigma(J_{P_{3_1}}) = \left\{ z \in \mathbb{C} : z = \Phi + \Psi \exp(\iota\theta) + \Omega \exp(2\iota\theta) + \Theta \exp(3\iota\theta),\ \iota^2 = -1,\ \theta \in \mathbb{R} \right\},$$

where

$$\begin{aligned} \Phi &= h_t'(x_{3_1}^*, x_{3_1}^*, x_{3_1}^*, x_{3_1}^*), \\ \Psi &= h_z'(x_{3_1}^*, x_{3_1}^*, x_{3_1}^*, x_{3_1}^*), \\ \Omega &= h_y'(x_{3_1}^*, x_{3_1}^*, x_{3_1}^*, x_{3_1}^*), \\ \Theta &= h_x'(x_{3_1}^*, x_{3_1}^*, x_{3_1}^*, x_{3_1}^*). \end{aligned}$$

Additionally, the 3-cycle P_{3_1} satisfies the following stability conditions:

1. *Asymptotically stable if $|\Phi| + |\Psi| + |\Omega| + |\Theta| < 1$,*
2. *Unstable if $|\Phi| + |\Psi| + |\Omega| + |\Theta| > 1$,*
3. *Repulsive if $\left||\Phi| - |\Psi| + |\Omega| - |\Theta|\right| > 1$.*

Proof. From the definition of the Jacobian matrix $J_{P_{3_1}}$ associated with the 3-periodic point, $J_{P_{3_1}}$ can be expressed in the following block-diagonal form:

$$J_{P_{3_1}} = \begin{pmatrix} \ddots & \ddots & \vdots & \vdots & \vdots & \vdots & \ddots \\ \ddots & \ddots & 0 & \vdots & \vdots & \vdots & \ddots \\ \ddots & \ddots & \Phi & 0 & \vdots & \vdots & \ddots \\ \ddots & \ddots & \Psi & [\Phi] & 0 & \vdots & \ddots \\ \ddots & \ddots & \Omega & \Psi & \Phi & \ddots & \ddots \\ \ddots & \ddots & \Theta & \Omega & \Psi & \ddots & \ddots \\ \ddots & \vdots & 0 & \Theta & \Omega & \ddots & \ddots \\ \ddots & \vdots & \vdots & 0 & \Theta & \ddots & \ddots \\ \ddots & \vdots & \vdots & \vdots & 0 & \ddots & \ddots \\ \ddots & \vdots & \vdots & \vdots & \vdots & \ddots & \ddots \end{pmatrix}.$$

Using this structure, $J_{P_{3_1}}$ can be rewritten as

$$J_{P_{3_1}} = \Phi \cdot I + \Psi \cdot S + \Omega \cdot S^2 + \Theta \cdot S^3,$$

where Φ, Ψ, Ω, and Θ are defined as in the theorem, I denotes the identity operator, and S denotes the shift operator on the Hilbert space X. According to the polynomial spectral mapping theorem (see [26, Theorem 1, p. 53]), the spectrum of $J_{P_{3_1}}$ is given by

$$\sigma(J_{P_{3_1}}) = \Phi \cdot \sigma(I) + \Psi \cdot \sigma(S) + \Omega \cdot \sigma(S)^2 + \Theta \cdot \sigma(S)^3,$$

This corresponds to the formula for $\sigma(J_{P_{3_1}})$ provided in the theorem, i.e.

$$\sigma(J_{P_{3_1}}) = \left\{ z \in \mathbb{C} : z = \Phi + \Psi \exp(\iota\theta) + \Omega \exp(2\iota\theta) + \Theta \exp(3\iota\theta),\ \iota^2 = -1,\ \theta \in \mathbb{R} \right\}.$$

Furthermore, the spectral radius of $J_{P_{3_1}}$ is

$$\sup\{|\lambda| : \lambda \in \sigma(J_{P_k})\} = |\Phi| + |\Psi| + |\Omega| + |\Theta|,$$

and the minimum spectral radius is

$$\inf\{|\lambda| : \lambda \in \sigma(J_{P_k})\} = \inf\left\{|z| : z = \Phi + \Psi\exp(\iota\theta) + \Omega\exp(2\iota\theta) + \Theta\exp(3\iota\theta),\ \iota^2 = -1,\ \theta \in \mathbb{R}\right\}$$

Based on the spectral radius and the minimum spectral radius, the stability criteria (asymptotic stability, instability, and repulsiveness) directly follow from Theorem 1. □

2.3. Bifurcation analysis

Consider the dynamics described by Eqs (1.1)–(1.4), which depend on two real parameters a and b. Let J_{P_k} denote the Jacobian matrix of the map F^k at a k-cycle P_k. The k-th order bifurcation curves Λ^{P_k} in the (a, b) parameter plane are defined by the following system:

$$\begin{cases} \sigma(J_{P_k}) \cap \mathbb{S}(0,1) = S, \\ \Lambda^{P_k} = \{(a,b) \in \mathbb{R}\times\mathbb{R} : S \neq \emptyset\}. \end{cases}$$

For specific configurations of the multiplier set $S \subset \mathbb{C}$, the following classical cases of bifurcation curves can be distinguished (as described in [27, 28]):

- Fold bifurcation curve $\Lambda^{P_k}_{(k)_0}$: This corresponds to parameter points $(a, b) \in \mathbb{R}\times\mathbb{R}$ where $S = \{+1\}$ for a k-cycle.
- Flip bifurcation curve $\Lambda^{P_k}_{k}$: This corresponds to parameter points $(a, b) \in \mathbb{R}\times\mathbb{R}$ where $S = \{-1\}$ for a k-cycle $P_k \in X$.

3. Study of a spatiotemporal quadratic map

In [29], the author asks some questions concerning noninvertible "spatio-discrete temporal" maps, and considers the following spatiotemporal quadratic map:

$$x_{m+1,n+1} := f(x_{m,n}, x_{m+1,n}) = x^2_{m,n} + bx_{m+1,n} + a. \tag{3.1}$$

This map is of significant importance as it can serve as a fundamental building block for understanding nonlinear cases, similar to the role played by the logistic map.

In the following, we recall some results stated in the paper [23] concerning the existence of fixed points of type 1_1 and 1_2 in addition to the 2-periodic points of type 2_1 for the 2D spatiotemporal discrete system (3.1), depending on the variation of the parameters in the (a, b)-plane.

Furthermore, we examine various bifurcation scenarios that can arise in relation to this quadratic map. These bifurcations correspond to changes in the dynamic behavior of system (3.1) as the parameters a and b are varied.

The 2D bifurcation diagram Figure 6 represents the stability zones of the fixed point of type 1_1 (noted P_{1_1}) in red, the fixed point of type 1_2 (noted P_{1_2}) in green, and the 2-periodic point of type 2_1 (noted P_{2_1}) in blue. The diagram is plotted in the (a, b)-parameter plane, where the values of the parameters a and b are varied.

By examining this bifurcation diagram, one can observe how the stability regions of these points change as the parameters a and b are adjusted. It provides insights into the parameter ranges where each point exhibits stability or undergoes bifurcations, allowing for a visual representation of the system's dynamics in the (a, b)-parameter space.

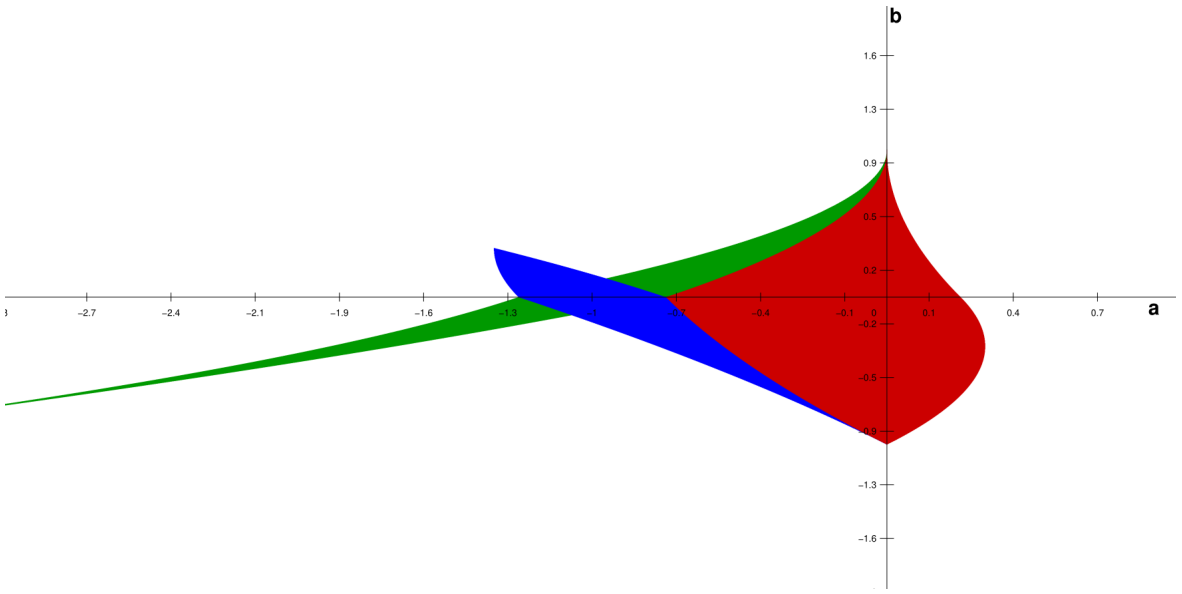

Figure 6. 2*D* Bifurcation diagram represented by the stability zones in the (a, b)-parameter plane. Within this diagram, different regions are colored to indicate the stability properties of the corresponding points. The red region represents the stability zone of the fixed point P_{1_1}, the green region indicates the stability zone of the fixed point P_{1_2}, and the blue region represents the stability zone of the 2-periodic point P_{2_1}.

3.1. Reminder of some results on cycles 1 and 2

As the parameters a and b vary across the set of real numbers, the map (3.1) can exhibit various equilibrium solutions. These equilibrium solutions correspond to the fixed points and 2-cycles listed in Remark 1.

Depending on the specific values of a and b, the map (3.1) may possess stable fixed points or periodic orbits. These equilibrium solutions can be identified by analyzing the stability properties of the map at different parameter values. It is important to note that the specific behavior of the map (3.1) and the occurrence of equilibrium solutions may depend on the functional form and properties of the map itself, as well as the specific values of the parameters a and b. Further analysis and numerical investigation may be required to determine the precise equilibrium solutions and their stability characteristics for different parameter values within the real number range.

3.1.1. Fixed points of type 1_1

For $b^2 - 2b + 1 - 4a \geq 0$, the map (3.1) has two fixed points of type 1_1, given by

$$P_{1_1} = (x_i = x^*_{1_1})_{i=-\infty}^{\infty} \quad \text{and} \quad P'_{1_1} = (x_i = x^{**}_{1_1})_{i=-\infty}^{\infty},$$

where

$$x^*_{1_1} = -\frac{1}{2}b + \frac{1}{2} - \frac{1}{2}\sqrt{b^2 - 2b + 1 - 4a}, \quad x^{**}_{1_1} = -\frac{1}{2}b + \frac{1}{2} + \frac{1}{2}\sqrt{b^2 - 2b + 1 - 4a}.$$

3.1.2. Fixed points of type 1_2

For $-3b^2 + 6b - 3 - 4a \geq 0$, the map (3.1) has two fixed points of type 1_2, expressed as

$$P_{1_2} = (x_{2i} = x^*_{1_2},\ x_{2i+1} = y^*_{1_2})_{i=-\infty}^{\infty} \quad \text{and} \quad P'_{1_2} = (x_{2i} = y^*_{1_2},\ x_{2i+1} = x^*_{1_2})_{i=-\infty}^{\infty},$$

where

$$\begin{cases} x^*_{1_2} = -\dfrac{1}{2} + \dfrac{1}{2}b - \dfrac{1}{2}\sqrt{-3b^2 + 6b - 3 - 4a}, \\ \\ y^*_{1_2} = -\dfrac{1}{2} + \dfrac{1}{2}b + \dfrac{1}{2}\sqrt{-3b^2 + 6b - 3 - 4a}. \end{cases}$$

3.1.3. Periodic point of period 2 of type 2_1

For $-3 - 2b + b^2 - 4a \geq 0$, the map (3.1) has a 2-periodic orbit $\{P_{2_1}, P'_{2_1}\}$ of type 2_1, represented by

$$P_{2_1} = (x_i = x^*_{2_1})_{i=-\infty}^{\infty} \quad \text{and} \quad P'_{2_1} = (y_i = y^*_{2_1})_{i=-\infty}^{\infty},$$

where

$$\begin{cases} x^*_{2_1} = -\dfrac{1}{2} - \dfrac{1}{2}b + \dfrac{1}{2}\sqrt{-3 - 2b + b^2 - 4a}, \\ \\ y^*_{2_1} = -\dfrac{1}{2} - \dfrac{1}{2}b - \dfrac{1}{2}\sqrt{-3 - 2b + b^2 - 4a}. \end{cases}$$

In Figure 6, each colored region corresponds to the existence of at least one stable singularity of the map f for specific values of the parameters a and b. The red region indicates a stable fixed point of type 1_1, the green region signifies a stable fixed point of type 1_2, and the blue region represents the presence of an attractive 2-periodic orbit $\{P_{2_1}, P'_{2_1}\}$. Conversely, the white region signifies the absence of stable cycles among these singularities. The analytically derived (a, b)-parametric plane shown in Figure 6 follows the methodology described in references [23, 24].

3.1.4. Bifurcation curves

The analytical studies presented in [23–25] allow for the determination of bifurcation curves in the (a, b)-plane that correspond to the fixed points of types 1_1 and 1_2, as well as the 2-cycle of type 2_1 in the quadratic map defined by equation (3.1). These references, particularly [23, 24], offer detailed results and insights into the nature of these bifurcations.

The analytical expressions provided in these works precisely describe the locations and shapes of the bifurcation curves in the (a, b)-plane. These curves demarcate regions where the stability of fixed points and periodic orbits undergo qualitative changes as the parameters a and b are varied.

Theorem 3. *Let $P_{1_1} = (x_i = x^*_{1_1})_{i=-\infty}^{i=\infty}$ be a fixed point of type 1_1 for the map (3.1) . Then:*

1. *The fold bifurcation curve associated with the fixed point P_{1_1}, denoted by $\Lambda^{P_{1_1}}_{(1)_0}$, is given in the (a, b)-plane by*
$$b \pm \left| b - 1 \pm \sqrt{b^2 - 4a - 2b + 1} \right| = 1.$$
2. *The flip bifurcation curve associated with the fixed point P_{1_1}, denoted by $\Lambda^{P_{1_1}}_{1}$, is given in the (a, b)-plane by*
$$b \pm \left| b - 1 \pm \sqrt{b^2 - 4a - 2b + 1} \right| = -1.$$

Proof. Let $A := f'_y(x^*_{1_1}, x^*_{1_1}) = b$ and $B := f'_x(x^*_{1_1}, x^*_{1_1}) = -b + 1 - \sqrt{b^2 - 4a - 2b + 1}$. The Jacobian matrix $J_{P_{1_1}}$ at P_{1_1} is
$$J_{P_{1_1}} = A \cdot I + B \cdot S,$$
where S is the shift operator [30, 31]. According to the polynomial spectral mapping theorem (see Theorem 1, p. 53, in Halmos [26]), the spectrum of $J_{P_{1_1}}$ is
$$\sigma(J_{P_{1_1}}) = A \cdot \sigma(I) + B \cdot \sigma(S).$$
Here, $\sigma(I) = \{A\}$ and $\sigma(S) = \{z \in \mathbb{C} : |z| = 1\}$ (see [30, 31]), so
$$\sigma(J_{P_{1_1}}) = \{z \in \mathbb{C} : z = A + B\exp(\iota\theta),\ \theta \in \mathbb{R}\}.$$
Using the bifurcation conditions, $S = \{+1\}$ for fold bifurcations, and $S = \{-1\}$ for flip bifurcations, as outlined in Section 3.4, the equations for the bifurcation curves are derived as
$$b \pm \left| b - 1 \pm \sqrt{b^2 - 4a - 2b + 1} \right| = 1 \quad \text{(fold bifurcation)},$$
and
$$b \pm \left| b - 1 \pm \sqrt{b^2 - 4a - 2b + 1} \right| = -1 \quad \text{(flip bifurcation)}.$$
This completes the proof. □

Theorem 4. *Let $P_{1_2} = (x_{2i} = x^*_{1_2}, x_{2i+1} = y^*_{1_2})_{i=-\infty}^{i=\infty}$ be a fixed point of type 1_2 for the map (3.1). Then:*

1. *The fold bifurcation curve associated with P_{1_2}, denoted by $\Lambda^{P_{1_2}}_{(1)_0}$, is given in the (a, b)-plane by*
$$b \pm \sqrt{\left| \left(-1 + b + \sqrt{-3b^2 - 4a + 6b - 3}\right)\left(-1 + b - \sqrt{-3b^2 - 4a + 6b - 3}\right) \right|} = 1.$$
2. *The flip bifurcation curve associated with P_{1_2}, denoted by $\Lambda^{P_{1_2}}_{1}$, is given in the (a, b)-plane by*
$$b \pm \sqrt{\left| \left(-1 + b + \sqrt{-3b^2 - 4a + 6b - 3}\right)\left(-1 + b - \sqrt{-3b^2 - 4a + 6b - 3}\right) \right|} = -1.$$

Proof. Let $A := f'_y(x^*_{1_2}, y^*_{1_2}) = b$, $B := f'_x(x^*_{1_2}, y^*_{1_2}) = -b+1+\sqrt{b^2-4a-2b+1}$, and $B' := f'_x(y^*_{1_2}, x^*_{1_2}) = -b+1-\sqrt{b^2-4a-2b+1}$. The Jacobian matrix $J_{P_{1_2}}$ is given by

$$J_{P_{1_2}} = AI + S_{BB'},$$

where $S_{BB'}$ is a weighted shift [26, 31] with weight (... , B' , (B) , B', ...). According to Theorem 6, p.6 in [23, 25], we have

$$\sigma(J_{P_{1_2}}) = \{z \in \mathbb{C} \,:\, |z| = R_1 \quad \vee \quad |z| = R_2\}\,.$$

where

$$R_1 = \left| b + \sqrt{\left(-b+1+\sqrt{b^2-4a-2b+1}\right)\left(-b+1-\sqrt{b^2-4a-2b+1}\right)}\mathrm{e}^{\iota\theta} \right|,\ \theta \in [0\,,\,2\pi),$$

and

$$R_2 = \left| b - \sqrt{\left(-b+1+\sqrt{b^2-4a-2b+1}\right)\left(-b+1-\sqrt{b^2-4a-2b+1}\right)}\mathrm{e}^{\iota\theta} \right|,\ \theta \in [0\,,\,2\pi).$$

and the bifurcation equations follow from the conditions for the fold and flip bifurcations applied to the quadratic system (3.1). □

Theorem 5. *Let P_{2_1} be a 2-cycle of type 2_1. Then:*

1. *The fold bifurcation curve associated with the 2-cycle $P_{2_1} = (x_i = x^*_{2_1})_{i=-\infty}^{i=\infty}$, denoted by $\Lambda^{P_{2_1}}_{(2)_0}$, is given in the (a, b)-plane by the equation*

$$\pm\left|\frac{\partial f^{[2]}(x,y,z)}{\partial x}\bigg|_{(x^*_{2_1},x^*_{2_1},x^*_{2_1})}\right| \pm \left|\frac{\partial f^{[2]}(x,y,z)}{\partial y}\bigg|_{(x^*_{2_1},x^*_{2_1},x^*_{2_1})}\right| \pm \left|\frac{\partial f^{[2]}(x,y,z)}{\partial z}\bigg|_{(x^*_{2_1},x^*_{2_1},x^*_{2_1})}\right| = +1, \qquad (3.2)$$

2. *The flip bifurcation curve associated with the 2-cycle P_{2_1}, denoted by $\Lambda^{P_{2_1}}_{2}$, is given in the (a, b)-plane by the equation*

$$\pm\left|\frac{\partial f^{[2]}(x,y,z)}{\partial x}\bigg|_{(x^*_{2_1},x^*_{2_1},x^*_{2_1})}\right| \pm \left|\frac{\partial f^{[2]}(x,y,z)}{\partial y}\bigg|_{(x^*_{2_1},x^*_{2_1},x^*_{2_1})}\right| \pm \left|\frac{\partial f^{[2]}(x,y,z)}{\partial z}\bigg|_{(x^*_{2_1},x^*_{2_1},x^*_{2_1})}\right| = -1. \qquad (3.3)$$

Proof. Let P_{2_1} be a 2-cycle of type 2_1, given by $P_{2_1} = (x_i = x^*_{2_1})_{i=-\infty}^{\infty}$. By definition, the 2-cycle P_{2_1} is a fixed point of the second iterate map F^2, and the Jacobian matrix $J_{P_{2_1}}$ of F^2 at P_{2_1} can be written as

$$J_{P_{2_1}} = \begin{pmatrix} \ddots & \ddots & \vdots & \vdots & \vdots & \vdots & \vdots \\ \ddots & \ddots & 0 & 0 & 0 & 0 & \cdots \\ \ddots & B & A & 0 & 0 & 0 & \cdots \\ \ddots & C & B & [A] & 0 & 0 & \cdots \\ \cdots & 0 & C & B & A & 0 & \cdots \\ \cdots & 0 & 0 & C & \ddots & \ddots & \ddots \\ \vdots & \vdots & \vdots & \ddots & \ddots & \ddots & \ddots \end{pmatrix},$$

where $A := \left.\frac{\partial f^{[2]}(x,y,z)}{\partial z}\right|_{(x^*_{2_1},x^*_{2_1},x^*_{2_1})}$, $B := \left.\frac{\partial f^{[2]}(x,y,z)}{\partial y}\right|_{(x^*_{2_1},x^*_{2_1},x^*_{2_1})}$, and $C := \left.\frac{\partial f^{[2]}(x,y,z)}{\partial x}\right|_{(x^*_{2_1},x^*_{2_1},x^*_{2_1})}$.

The Jacobian matrix $J_{P_{2_1}}$ can then be expressed as

$$J^*_{F^{[2]}} = A \cdot I + B \cdot S + C \cdot S^2,$$

where S is the shift operator. According to the polynomial spectral mapping theorem, the spectrum of $J_{P_{2_1}}$ is given by

$$\sigma(J_{P_{2_1}}) = A \cdot \sigma(I) + B \cdot \sigma(S) + C \cdot \sigma(S^2),$$

where $\sigma(I) = \{A\}$ and $\sigma(S) = \{z \in \mathbb{C} : |z| = 1\}$. Hence, the spectrum becomes

$$\sigma(J_{P_{2_1}}) = \{z \in \mathbb{C} : z = A + B\exp(i\theta) + C\exp(2i\theta),\ \theta \in \mathbb{R}\}.$$

For the fold bifurcation, the condition $S = \{1\}$ leads to the equation

$$\pm|A| \pm |B| \pm |C| = 1,$$

which corresponds to the fold bifurcation curve

$$\pm\left|\left.\frac{\partial f^{[2]}(x,y,z)}{\partial x}\right|_{(x^*_{2_1},x^*_{2_1},x^*_{2_1})}\right| \pm \left|\left.\frac{\partial f^{[2]}(x,y,z)}{\partial y}\right|_{(x^*_{2_1},x^*_{2_1},x^*_{2_1})}\right| \pm \left|\left.\frac{\partial f^{[2]}(x,y,z)}{\partial z}\right|_{(x^*_{2_1},x^*_{2_1},x^*_{2_1})}\right| = 1.$$

For the flip bifurcation, the condition $S = \{-1\}$ leads to the equation

$$\pm C \pm |B| \pm |A| = -1,$$

which corresponds to the flip bifurcation curve

$$\pm\left|\left.\frac{\partial f^{[2]}(x,y,z)}{\partial x}\right|_{(x^*_{2_1},x^*_{2_1},x^*_{2_1})}\right| \pm \left|\left.\frac{\partial f^{[2]}(x,y,z)}{\partial y}\right|_{(x^*_{2_1},x^*_{2_1},x^*_{2_1})}\right| \pm \left|\left.\frac{\partial f^{[2]}(x,y,z)}{\partial z}\right|_{(x^*_{2_1},x^*_{2_1},x^*_{2_1})}\right| = -1.$$

□

In Figure 7a, the stability region of the fixed point P_{2_1} (highlighted in red) is enclosed by the curves $\Lambda_1^{P_{1_1}}$ and $\Lambda_{(1)_0}^{P_{1_1}}$. Similarly, the stability region of the fixed point P_{1_2} (depicted in green) is bounded by the curves $\Lambda_{(1)_0}^{II}$ and Λ_1^{II}.

Notably, in the region Δ, bounded on the left by the curve $\Lambda_{(1)_0}^{P_{1_1}}$, no cycles exist. Upon crossing the curve $\Lambda_{(1)_0}^{P_{1_1}}$ from region Δ, the spectrum $\sigma(J_{P_{1_1}})$ of the Jacobian matrix at the fixed point P_{1_1} passes through the value 1. This transition induces a tangent bifurcation, resulting in the birth of a 2-cycle of type 2_1.

Similarly, in the region between $\Lambda_{(1)_0}^{P_{1_2}}$ and $\Lambda_1^{P_{1_2}}$, bounded on the right by $\Lambda_{(1)_0}^{P_{1_2}}$, the spectrum of the Jacobian matrix $J_{P_{1_2}}$ passes through the value -1. This crossing results in a flip bifurcation, leading to the creation of a 2-cycle of type 2_1.

In Figure 7b, the stability region of the 2-periodic point P_{2_1} is delimited by the curves ${}^1\Lambda_2^{P_{2_1}}$, ${}^2\Lambda_2^{P_{2_1}}$, ${}^1\Lambda_{(2)_0}^{P_{2_1}}$, ${}^2\Lambda_{(2)_0}^{P_{2_1}}$, ${}^3\Lambda_{(2)_0}^{P_{2_1}}$, and ${}^4\Lambda_{(2)_0}^{P_{2_1}}$. When the spectrum $\sigma(J_{P_{2_1}})$ crosses the value 1, it leads to bifurcations

characterized by the union of curves ${}^1\Lambda_{(2)_0}^{P_{2_1}} \cup {}^2\Lambda_{(2)_0}^{P_{2_1}} \cup {}^3\Lambda_{(2)_0}^{P_{2_1}} \cup {}^4\Lambda_{(2)_0}^{P_{2_1}}$, as described by Eq (3.2). Similarly, the bifurcations corresponding to the spectrum reaching -1 are characterised by the curves ${}^1\Lambda_{(2)_0}^{P_{2_1}} \cup {}^2\Lambda_{(2)_0}^{P_{2_1}} \cup {}^3\Lambda_{(2)_0}^{P_{2_1}} \cup {}^4\Lambda_{(2)_0}^{P_{2_1}}$, derived from equation (3.3). Similarly, the bifurcation curves corresponding to the spectrum reaching -1 are defined by ${}^1\Lambda_2^{P_{2_1}} \cup {}^2\Lambda_2^{P_{2_1}}$, derived from Eq (3.3).

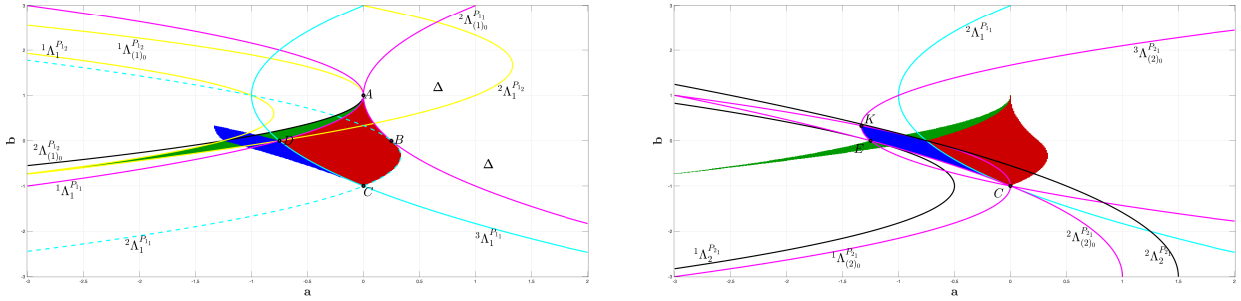

(a) Bifurcation curves for fixed points of type $1_{1,2}$. **(b)** Bifurcation curves for the 2-cycle of type 2_1.

Figure 7. First and second bifurcation curves of system (3.1).

Remark 4. *In Figure 7a, the singular points A and B correspond to cases where a fold bifurcation curve* $\Lambda_{(1)_0}^{P_{1_1}}$ *is tangent to a Flip bifurcation curves* ${}^{1,2}\Lambda_1^{P_{1_1}}$*. At these points, the multipliers satisfy* $S_1 = -S_2 = \{1\}$*, indicating a co-dimension-2 bifurcation. Points C and D have distinct origins: Point C results from the intersection of two flip bifurcation curves* ${}^2\Lambda_1^{P_{1_1}}$ *and* ${}^3\Lambda_1^{P_{1_1}}$ *where* $S_1 = S_2 = \{-1\}$*. Point D, however, emerges from the intersection of a fold bifurcation curve* $\Lambda_{(2)_0}^{P_{2_1}}$ *with a flip bifurcation curve* ${}^1\Lambda_1^{P_{1_1}}$ *where* $S_1 = -S_2 = \{1\}$*. All other intersections are solely caused by the projection of the bifurcation curves onto the* (a, b)*-plane.*

As indicated in Figure 7a the singular point C shown in Figure 7b involves, in addition to the bifurcation curves ${}^2\Lambda_1^{P_{1_1}}$ *of the 1-cycle, the fold bifurcation curves of the 2-cycle,* ${}^{1,2,3}\Lambda_{(2)_0}^{P_{2_1}}$*. At the singular point K, we observe the intersection of the fold bifurcation curves of the 2-cycle,* ${}^1\Lambda_{(2)_0}^{P_{2_1}}$ *and* ${}^2\Lambda_{(2)_0}^{P_{2_1}}$*. The singular point E is of codimension greater than 3; it arises from the intersection of three bifurcation curves: The flip bifurcation of a 1-cycle,* ${}^1\Lambda_1^{P_{1_1}}$*, and the two Fold bifurcation curves of the 2-cycle,* ${}^2\Lambda_{(2)_0}^{P_{2_1}}$ *and* ${}^3\Lambda_{(2)_0}^{P_{2_1}}$*. The multipliers at this point satisfy* $S_1 = -S_2 = \{1\}$*. All other intersections are solely due to the projection of bifurcation curves onto the* (a, b)*-plane.*

3.2. Existence of 3-cycles of the spatiotemporal quadratic map

The presence of a period-3 cycle in the logistic function has been well-established (see [32–35]). This finding suggests the existence of even longer periodic orbits [29, 33]. The period-doubling route to chaos, a well-known phenomenon, is demonstrably dependent on the control parameter's strength.

Setting $b = 0$ in system (3.1) reduces it to the quadratic recurrence $x_{n+1} = x_n^2 + a$. In the bifurcation diagram (Figure 8a), the 3-period window of the quadratic map near $a = -1.7660$ is displayed. Similarly, if b is close to 0, for example, $b = 0.02$, could system (3.1) exhibit the same behavior?

Effectively, for $b = 0.02$ and $a \in [-1.8, -1.7]$, the dynamics of system (3.1) reveal a period-3 window, followed by a sequence of chaotic regimes (see Figure 8). This transition is marked by the emergence of a chaotic attractor, which arises after the destabilization of the 3-cycle of type 3_1, as illustrated in Figure 9. In the remainder of this paper, we provide a detailed exposition of the existence of 3-cycles of different types, along with a stability and bifurcation analysis, including a geometric study of the foliation structure within the (a, b)-parameter plane.

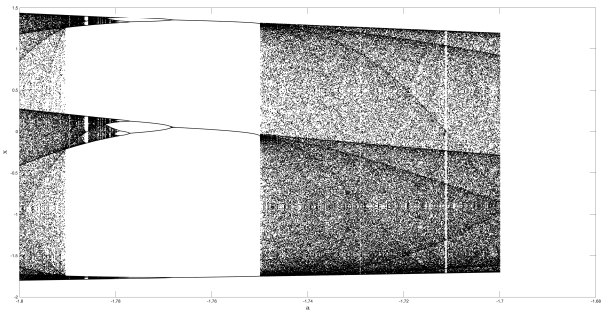

(a) Bifurcation diagram of the 1-D map $x_{n+1} = x_n^2 + a$ versus parameter $a \in [-1.8, -1.7]$. The attracting 3-cycles appear in the window $a \in (-1.77, -1.750)$.

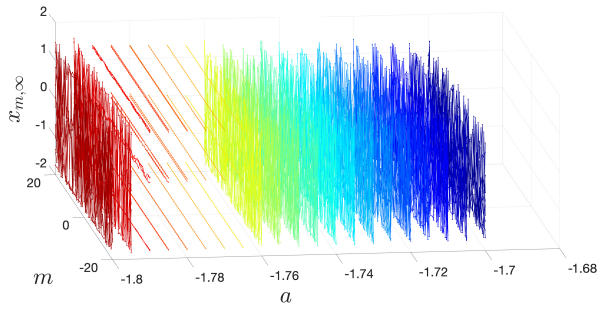

(b) Bifurcation diagram of system (3.1) versus b, for $b = 0.02$ and $a \in [-1.8, -1.7]$. We observe the emergence of 3-cycles of type 3_2 characterized by the coexistence of two distinct values on the same line.

Figure 8. Bifurcation diagram of system (3.1).

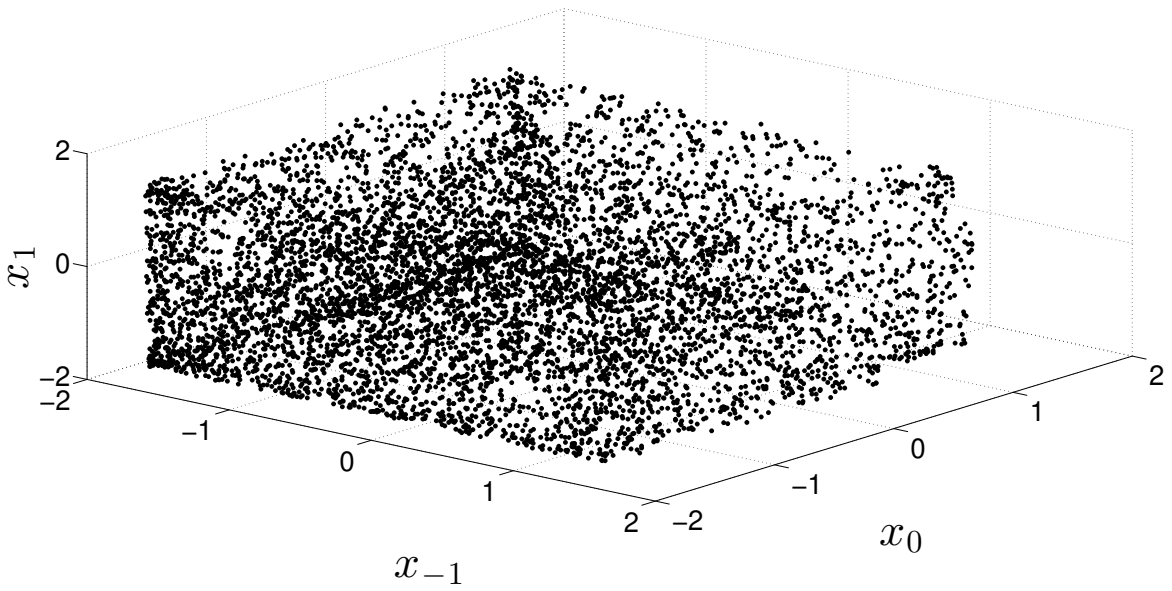

Figure 9. Projection of the attractive strange attractor on (x_{-1}, x_0, x_1)-space, after destabilization of stable 3-cycle 3_1 when $a = -1.7660$ and $b = 0.05$.

3.2.1. Case of 3-cycles of type 3_1 (H type)

A 3-cycle of type 3_1 is a solution to the equation $h(x,x,x,x) - x = 0$ where $f(x^*, x^*) \neq x^*$. The polynomial $h(x,x,x,x) - x$ has degree 8 and is divisible by $f(x,x) - x$. Defining $Q(X)$ as the quotient of these two expressions gives a polynomial of degree 6, given by

$$\begin{aligned} Q(X) = (1 + b + b^2 + a + 3ab + b^2a + 2a^2 + 2ba^2 + a^3) \\ +(1 + 2b + 2b^2 + b^3 + 2a + 4ab + 4b^2a + a^2 + 3ba^2)X \\ +(1 + 3b + 3b^2 + 2b^3 + 3a + 6ab + 3b^2a + 3a^2)X^2 \\ +(1 + 3b + 5b^2 + b^3 + 2a + 6ab)X^3 \\ +(1 + 4b + 3b^2 + 3b)X^4 \\ +(1 + 3b)X^5 + X^6. \end{aligned}$$

If x^* is a root of $h(x,x,x,x) - x$, then $y = f(x,x)$ is also a root. The polynomial Q has 6 roots, which form two 3-cycles of type 3_1.

When $b = 0.002$, $a = -1.766$, system (3.1) exhibits a stable 3-cycle of type 3_1 denoted P_{3_1} and given by $P_{3_1} = \left(x_i^* = -1.764267556\right)_{i=-\infty}^{\infty}$. The Jacobian matrix of $J_{P_{3_1}}$ can be obtained as (2.1)–(2.2), and the spectrum of the Jacobian matrix is given by

$$\sigma(J_{P_{3_1}}) = \Phi + \Psi e^{i\theta} + \Omega e^{2\,i\theta} + \Theta e^{3\,i\theta},$$

when the values of Φ, Ψ, Ω, and Θ are approximately $0.0, -0.3044171416 \times 10^{-5}, -0.01909377224$, and -0.7703056278, respectively, so the spectrum $\sigma(J_{P_{3_1}})$ lies inside the unit disk. Therefore, the 3-cycle P_{3_1} is stable for the value $a = -1.766$ (as depicted in Figure 10a–10b), followed by a sequence of stable/unstable regimes. It is worth noting that the 3-cycle P_{3_1} becomes destabilized and gives rise to a strange attractor when $a = -1.740$ (see Figure 9). On the other hand, an unstable 3-cycle orbit of type 3_1 for system (3.1) is given by

$$P'_{3_1} = (x_i = -1.74328)_{i=-\infty}^{\infty} \mapsto (x_i = 1.26954)_{i=-\infty}^{\infty} \mapsto (x_i = -0.151736)_{i=-\infty}^{\infty} \mapsto P'_{3_1}.$$

The Jacobian matrix of $J_{P'_{3_1}}$ can be derived using Eqs (2.1)–(2.2), and its spectrum its given by

$$\sigma(J_{P'_{3_1}}) = \Phi + \Psi e^{i\theta} + \Omega e^{2\,i\theta} + \Theta e^{3\,i\theta},$$

when the values of Φ, Ψ, Ω, and Θ are approximately $0.0, -0.0004864819978, -0.1732908362$, and 2.246615678, respectively, so the spectrum $\sigma(J_{P'_{3_1}})$ lies outside the unit disk (see Figure 11).

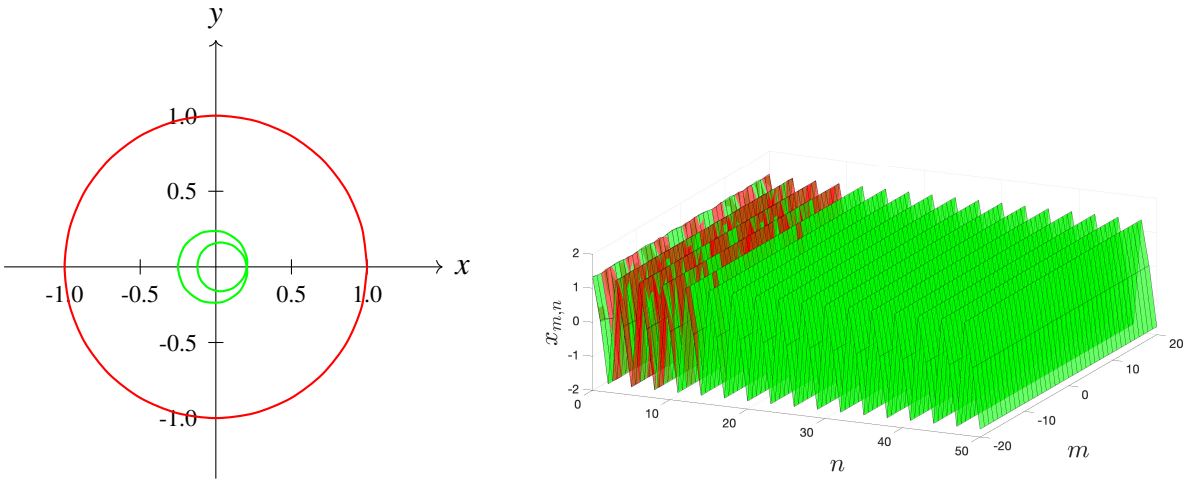

(a) (b)

Figure 10. Behavior of the solutions near the 3-cycle P_{3_1} of the 2D spatiotemporal discrete system (3.1) when $b = 0.02$ and $a = -1.766$. (a) The red line corresponds to the unit circle $\mathbb{S}(0, 1)$, and in green the spectrums of the Jacobian of the system (3.1) evaluated at the 3_1-cycle, P_{3_1}. (b) The behavior and stability of the solution within the 3-cycle P_{3_1} is stable when $b = 0.02$ and $a = -1.74$.

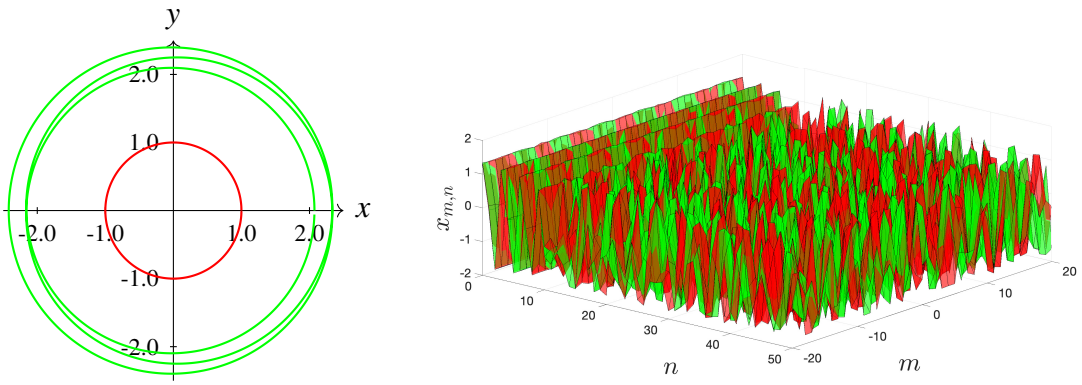

(a) (b)

Figure 11. Behavior of the solutions near the 3-cycle P'_{3_1} of the 2D spatiotemporal discrete system (3.1) when $b = 0.02$ and $a = -1.74$. (a) The red line corresponds to the unit circle $\mathbb{S}(0, 1)$, and in green the spectrums of the Jacobian of the system (3.1) evaluated at the 3-cycle, P'_{3_1}. (b) The behavior and instability of the solution within the 3-cycle P'_{3_1} when $b = 0.02$ and $a = -1.74$.

3.3. Restriction of the study on space X_3

Analytically characterizing the stability of 3-cycles other than type 3_1 is challenging. Hence, we have limited the study of stability to the space X_3, defined as

$$X_3 := \left\{[x] := (x_{3i} = x, x_{3i+1} = y, x_{3i+2} = z)_{i=-\infty}^{\infty} \in \mathbb{R}^{\mathbb{Z}}; (x, y, z) \in \mathbb{R}^3\right\} \subset X.$$

Since we consider only 3-cycles, we can construct a new Jacobian matrix of dimension 3×3. Let us consider the function $G : \mathbb{R}^3 \to \mathbb{R}$ given by $G(x, y, z) := h(x, y, z, x)$. Then, we define the function $\widetilde{G} : \mathbb{R}^3 \to \mathbb{R}^3$ by:

$$\widetilde{G}(x, y, z) = \begin{pmatrix} G(x, y, z) \\ G(y, z, x) \\ G(z, x, y) \end{pmatrix}$$

A general 3-cycle is therefore a fixed point of type 1_1, (i.e., $\widetilde{G}(x, y, z) = (x, y, z)$) which is neither a 1-cycle nor a 2-cycle. The Jacobian matrix of $\widetilde{G}$ at $P_3 = (x_{3i} = x_1^*, x_{3i+1} = x_2^*, x_{3i+2} = x_3^*)_{i=-\infty}^{i=\infty}$ is

$$J_{P_3}^{(3)} = \begin{pmatrix} \frac{\partial G}{\partial x}(x_1^*, x_2^*, x_3^*) & \frac{\partial G}{\partial y}(x_1^*, x_2^*, x_3^*) & \frac{\partial G}{\partial z}(x_1^*, x_2^*, x_3^*) \\ \frac{\partial G}{\partial z}(x_2^*, x_3^*, x_1^*) & \frac{\partial G}{\partial x}(x_2^*, x_3^*, x_1^*) & \frac{\partial G}{\partial y}(x_2^*, x_3^*, x_1^*) \\ \frac{\partial G}{\partial y}(x_3^*, x_1^*, x_2^*) & \frac{\partial G}{\partial z}(x_3^*, x_1^*, x_2^*) & \frac{\partial G}{\partial x}(x_3^*, x_1^*, x_2^*) \end{pmatrix}$$

3.3.1. Study of 3-cycle of type 3_{3-} (AD Type)

The cycle of type 3_{3-}, denoted $P_{3_{3-}} = (x_{3i} = x^*, x_{3i+1} = y^*, x_{3i+2} = z^*)_{i=-\infty}^{\infty}$, is defined by the following system of equations:

$$\begin{cases} f(x^*, y^*) = z^*, \\ f(y^*, z^*) = x^*, \\ f(z^*, x^*) = y^*, \end{cases}$$

where $(x^*, y^*, z^*) \neq (x^*, x^*, x^*)$. In this case, the partial derivatives of $G(x^*, y^*, z^*)$ are given by

$$A := \partial_1 G(x^*, y^*, z^*) = \partial_1 f(x^*, y^*)\partial_1 f(y^*, z^*)\partial_1 f(z^*, x^*) + \partial_2 f(x^*, y^*)\partial_2 f(y^*, z^*)\partial_2 f(z^*, x^*),$$

$$\partial_2 G(x^*, y^*, z^*) = \partial_1 f(y^*, z^*)\left(\partial_1 f(x^*, y^*)\partial_2 f(y^*, z^*) + \partial_1 f(y^*, z^*)\partial_2 f(z^*, x^*) + \partial_1 f(z^*, x^*)\partial_2 f(x^*, y^*)\right).$$

Let $B := \partial_1 f(x^*, y^*)\partial_2 f(y^*, z^*) + \partial_1 f(y^*, z^*)\partial_2 f(z^*, x^*) + \partial_1 f(z^*, x^*)\partial_2 f(x^*, y^*)$. Then,

$$\partial_3 G(x^*, y^*, z^*) = \partial_2 f(y^*, z^*)\left(\partial_1 f(x^*, y^*)\partial_2 f(y^*, z^*) + \partial_1 f(y^*, z^*)\partial_2 f(z^*, x^*) + \partial_1 f(z^*, x^*)\partial_2 f(x^*, y^*)\right).$$

The Jacobian matrix for this cycle is

$$J^{(3)}_{P_{3_{3-}}} = \begin{pmatrix} A & B\times\partial_1 f(y,z) & B\times\partial_2 f(y,z) \\ B\times\partial_2 f(z,x) & A & B\times\partial_1 f(z,x) \\ B\times\partial_1 f(x,y) & B\times\partial_2 f(x,y) & A \end{pmatrix}.$$

The characteristic polynomial of the matrix $J^{(3)}_{P_{3_{3-}}}$ is

$$\chi(t) = -t^3 + t^2(3b^3 + 24xyz)$$
$$+t\left(-3b^6 + 8b^3x^3 + 24b^3x^2y + 24b^3xy^2 + 8b^3y^3 + 24b^3x^2z + 24b^3y^2z + 24b^3xz^2 + 24b^3yz^2 - 192x^2y^2z^2 + 8b^3z^3\right)$$
$$+b^9 + 24b^6xyz + 192b^3x^2y^2z^2 + 512x^3y^3z^3.$$

When $b = 0.002$ and $a = -1.766$, two anti-diagonal (3_{3-} type) 3-cycles are obtained, one of which is stable and the other unstable.

- The stable 3-cycle of type 3_{3-} is given by

$$P_{3_{3-}} = (x_{3i} = -1.76255, x_{3i+1} = 0.0277649, x_{3i+2} = 1.34063)_{i=-\infty}^{\infty}$$

The Jacobian matrix is

$$J^{(3)}_{P_{3_{3-}}} = \begin{pmatrix} -0.524851 & -0.0000875489 & -3.15322\times10^{-6} \\ -3.15322\times10^{-6} & -0.524851 & -0.0042273 \\ 0.0055577 & -3.15322\times10^{-6} & -0.524851 \end{pmatrix}$$

and the moduli of the eigenvalues are 0.525488, 0.525488, and 0.52358.

- The second 3-cycle of type 3_{3-} is unstable, and is given by

$$P_{3_{3-}} = (x_{3i} = -1.74471, x_{3i+1} = -0.136876, x_{3i+2} = 1.27774)_{i=-\infty}^{\infty}$$

The Jacobian matrix is

$$J^{(3)}_{P_{3_{3-}}} = \begin{pmatrix} 2.44108 & 0.000661216 & -4.83078\times10^{-6} \\ -4.83078\times10^{-6} & 2.44108 & -0.00617247 \\ 0.00842831 & -4.83078\times10^{-6} & 2.44108 \end{pmatrix}$$

and the moduli of the eigenvalues are 2.4427, 2.4427, and 2.43782.

The bifurcation occurs with $b = 0.002$ and $a \in (-1.755006, -1.755007)$. For the value $a = -1.755007$, we obtain

$$P_{3_{3-}} = (x_{3i} = -1.74939,\ x_{3i+1} = -0.0548529,\ x_{3i+2} = 1.30524)_{i=-\infty}^{\infty}.$$

The Jacobian matrix is

$$J^{(3)}_{P_{3_{3-}}} = \begin{pmatrix} 1.002 & 0.000218973 & -3.992\times10^{-6} \\ -3.992\times10^{-6} & 1.002 & -0.00521052 \\ 0.00698356 & -3.992\times10^{-6} & 1.002 \end{pmatrix}.$$

The absolute values of the eigenvalues are 1.002995493509572, 1.002995493509572, and 1.0000000000002065.

3.3.2. Study of 3-cycle of type 3_{3+} (D type)

The 3-cycle of type 3_{3+}, denoted by $P_{3_{3+}} = (x_{3i} = x^*, x_{3i+1} = y^*, x_{3i+2} = z^*)_{i=-\infty}^{\infty}$, is defined by the system of equations

$$f(x^*, y^*) = x^*, \quad f(y^*, z^*) = y^*, \quad f(z^*, x^*) = z^*,$$

with $(x^*, y^*, z^*) \neq (x^*, x^*, x^*)$. In this case, the partial derivatives of $G(x^*, y^*, z^*)$ are given by

$$\partial_1 G(x^*, y^*, z^*) = (\partial_1 f(x^*, y^*))^3 + \partial_2 f(x^*, y^*)\partial_2 f(y^*, z^*)\partial_2 f(z^*, x^*),$$
$$\partial_2 G(x^*, y^*, z^*) = \partial_2 f(x^*, y^*)\Big((\partial_1 f(x^*, y^*))^2 + \partial_1 f(x^*, y^*)\partial_1 f(y^*, z^*) + (\partial_1 f(y^*, z^*))^2\Big),$$
$$\partial_3 G(x^*, y^*, z^*) = \partial_2 f(x^*, y^*)\partial_2 f(y^*, z^*)\Big(\partial_1 f(x^*, y^*) + \partial_1 f(y^*, z^*) + \partial_1 f(z^*, x^*)\Big).$$

Let $A = \partial_1 f(x^*, y^*) + \partial_1 f(y^*, z^*) + \partial_1 f(z^*, x^*)$ and $B = \partial_2 f(x^*, y^*)\partial_2 f(y^*, z^*)\partial_2 f(z^*, x^*)$. Then, the Jacobian matrix for this 3-cycle is

$$J^{(3)}_{P_{3_{3+}}} = \begin{pmatrix} (\partial_1 f(x,y))^3 + B & \partial_2 f(x,y)\Big((\partial_1 f(x,y))^2 + \partial_1 f(x,y)\partial_1 f(y,z) + (\partial_1 f(y,z))^2\Big) & A \times \partial_2 f(x,y) \times \partial_2 f(y,z) \\ A \times \partial_2 f(y,z) \times \partial_2 f(z,x) & (\partial_1 f(y,z))^3 + B & \partial_2 f(y,z)\Big((\partial_1 f(y,z))^2 + \partial_1 f(y,z)\partial_1 f(z,x) + (\partial_1 f(z,x))^2\Big) \\ \partial_2 f(z,x)\Big((\partial_1 f(z,x))^2 + \partial_1 f(z,x)\partial_1 f(x,y) + (\partial_1 f(x,y))^2\Big) & A \times \partial_2 f(z,x) \times \partial_2 f(x,y) & (\partial_1 f(z,x))^3 + B \end{pmatrix}$$

For the function $f(x, y) = x^2 + by + a$, $P_{3_{3+}} = (x_{3i} = x^*, x_{3i+1} = y^*, x_{3i+2} = z^*)_{i=-\infty}^{\infty}$ is a 3-cycle of type 3_{3+} if and only if x^* (or y^* or z^*) is a root of the following degree 6 polynomial:

$$\begin{aligned} Q(X) = {} & 1 + \frac{1}{b^2} + \frac{1}{b} + \frac{a}{b^4} + \frac{3a}{b^3} + \frac{a}{b^2} + \frac{2a^2}{b^5} + \frac{2a^2}{b^4} + \frac{a^3}{b^6} \\ & + \left(-\frac{1}{b^4} - \frac{2}{b^3} - \frac{2}{b^2} - \frac{1}{a} - \frac{4b}{b^5} - \frac{4b}{b^4} - \frac{2a}{b^3} - \frac{3a^2}{b^6} - \frac{a^2}{b^5}\right)X \\ & + \left(\frac{2}{b^5} + \frac{3}{b^4} + \frac{3}{b^3} + \frac{1}{b^2} + \frac{3b}{b^6} + \frac{6b}{b^5} + \frac{3b}{b^4} + \frac{3b^2}{b^6}\right)X^2 \\ & + \left(-\frac{1}{b^6} - \frac{5}{b^5} - \frac{3}{b^4} - \frac{1}{b^3} - \frac{6b}{b^6} - \frac{2b}{b^5}\right)X^3 \\ & + \left(\frac{3}{b^6} + \frac{4}{b^5} + \frac{1}{b^4} + \frac{3a}{b^6}\right)X^4 \end{aligned}$$

$$+\left(-\frac{3}{b^6}-\frac{1}{b^5}\right)X^5+\frac{X^6}{b^6}.$$

For numerical calculations, with $b = 0.002$ and $a = -1.766$, we find two unstable 3_{3+} type cycles:

1. The first 3-cycle is given by $P_{3_{3+}} = (-0.920506, -0.918506, 1.92051)$. The Jacobian matrix is

$$J^{(3)}_{P_{3_{3+}}} = \begin{pmatrix} -6.23979 & 0.0202918 & 6.51964\times10^{-7} \\ 6.5196\times10^{-7} & -6.1992 & 0.022144 \\ 0.0221427 & 6.51964\times10^{-7} & 56.668 \end{pmatrix}$$

with eigenvalue moduli $56.668, 6.23978$, and 6.19921.

2. The second 3-cycle is $P_{3_{3+}} = (-0.918507, 1.91851, 1.92051)$. The Jacobian matrix is

$$J^{(3)}_{P_{3_{3+}}} = \begin{pmatrix} -6.19923 & 0.0220973 & 0.000023364 \\ 0.000023364 & 56.491 & 0.0884281 \\ 0.022144 & 0.000023364 & 56.6679 \end{pmatrix}$$

with eigenvalue moduli $56.6679, 56.491$, and 6.19923.

3.3.3. Analysis of the 3-cycle of type 3_2 (SD Type)

The standard definitions of cycles do not directly apply here due to the horizontal periodicity of order 2. To analyze the 3-cycle of type 3_2 (SD type), we use the following function:

$$\begin{aligned} H(x,y) &:= h(y,x,y,x) \\ &= \Big(\big(Bx+y^2+A\big)^2 + B\big(By+x^2+A\big)+A\Big)^2 + B\Big(\big(By+x^2+A\big)^2 + B\big(Bx+y^2+A\big)+A\Big)+A \end{aligned}$$

The system of equations defining the 3-cycle of type 3_2, denoted $P_{3_2} = (x_{2i} = x^*, x_{2i+1} = y^*)_{i=-\infty}^{\infty}$, is

$$H(x,y) = x, \quad H(y,x) = y$$

The Jacobian matrix at the 3-cycle P_{3_2} is given by

$$J^{(3)}_{P_{3_2}} = \begin{pmatrix} \frac{\partial H}{\partial x}(x^*,y^*) & \frac{\partial H}{\partial y}(x^*,y^*) \\ \frac{\partial H}{\partial y}(y^*,x^*) & \frac{\partial H}{\partial x}(y^*,x^*) \end{pmatrix}$$

Explicitly, it can be written as

$$J^{(3)}_{P_{3_2}} = \begin{pmatrix} 2(K^2+bM+a)(4Kx+b^2)+b(2bM+2bx) & 2(K^2+bM+a)(2bK+2by)+b(4My+b^2) \\ 2(M^2+bK+a)(2bM+2bx)+b(4Kx+b^2)(4My+b^2) & 2(M^2+bK+a)(4My+b^2)+b(2bK+2by) \end{pmatrix},$$

where $K = by + x^2 + a$ and $M = bx + y^2 + a$.

This type of 3-cycle appears in the bifurcation diagram (see Figure 8) near the parameter values $b = 0.02$ and $a = -1.794$. For $b = 0.02$ and $a = -1.766$, two stable 3_2-cycles and one unstable 3-cycle of type 3_2 are observed

1. First stable 3-cycle of type 3_2:

$$P_{3_2} = (x_{2i} = 0.1339723819, x_{2i+1} = -0.01012437968)_{i=-\infty}^{\infty}$$

The Jacobian matrix is

$$J_{P_{3_2}}^{(3)} = \begin{pmatrix} -0.1879415909 & -2.523212893 \\ 0.1997303233 & -0.2018565029 \end{pmatrix}$$

with eigenvalue modulus 0.7361.

2. Second stable 3-cycle of type 3_2:

$$P_{3_2} = (x_{2i} = -1.648223584, x_{2i+1} = -0.8105549453)_{i=-\infty}^{\infty}$$

The Jacobian matrix is

$$J_{P_{3_2}}^{(3)} = \begin{pmatrix} -0.02774776706 & -3.088383918 \\ 11.89855413 & 0.06822802353 \end{pmatrix}$$

with eigenvalue modulus 0.7361.

3. Unstable 3-cycle of type 3_2:

$$P_{3_2} = (x_{2i} = -1.485768592, x_{2i+1} = 0.8529672112)_{i=-\infty}^{\infty}$$

The Jacobian matrix is

$$J_{P_{3_2}}^{(3)} = \begin{pmatrix} -0.2422270957 & 8.341366323 \\ 4.367465416 & 0.06941206786 \end{pmatrix}$$

with eigenvalues having a modulus of 0.7361.

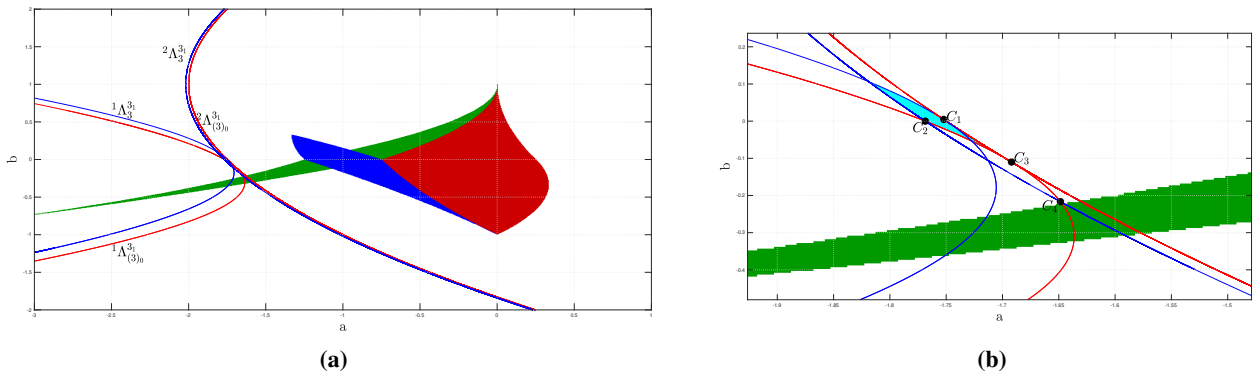

(a) **(b)**

Figure 12. Stability zones in (a, b)-parameter plane for fixed points. The red region represents the stability zone of the fixed point of type 1_1, the green region corresponds to the fixed point of type 1_2, and the blue region represents the 2-periodic point of type 2_1. The 3-cycles of type 3_1 are shown in cyan. The bifurcation curve for $S = \{+1\}$ of 3-cycles of type 3_1 is depicted as a solid blue line, while the curve for $S = \{-1\}$ is shown as a solid red line. In (b), magnification of a specific region in (a) displays detailed stability zones and fold bifurcation curves for 3-cycles of type 3_1.

3.4. Bifurcation analysis

Figure 12 illustrates the bifurcation diagram of the spatiotemporal quadratic map f in the (a, b) parameter plane for the 3_1-cycle in the case under consideration. The fold and flip bifurcations related to the fixed points of types 1_1 and 1_2 of f have already been analyzed in Section 3.1.1 (see also [23,24]). The definitions of fold and flip bifurcations are provided in Section 2.3. Specifically, in the (a, b) parameter plane, the flip bifurcation curves are denoted by ${}^{j}\Lambda_{3}^{3_1}$, where $j = 1, 2$, and the fold bifurcation curves are denoted by ${}^{j}\Lambda_{(3)_0}^{3_1}$, where $j = 1, 2$. The index j differentiates between curves associated with the same cycle. The blue region represents the stability region of the 3_1-cycle (see Figure 12a).

At the singular points C_i, for $i = 1, 2, 4$, the flip curves ${}^{j}\Lambda_{3}^{3_1}$ (for $j = 1, 2$) are tangent to the fold curves ${}^{j}\Lambda_{(3)_0}^{3_1}$ (for $j = 1, 2$). At these points, two of the multipliers are $S_1 = -S_2 = \{1\}$ (see, for example, [36]). At the singular point C_3, the fold curves ${}^{1}\Lambda_{(3)_0}^{3_1}$ and ${}^{2}\Lambda_{(3)_0}^{3_1}$ are tangential to each other (see Figure 12b).

The foliation of the parameter plane associated with the map f at the 3_1-cycle is qualitatively shown in Figure 13. A fold curve ${}^{1}\Lambda_{(3)_0}^{3_1}$ (respectively ${}^{2}\Lambda_{(3)_0}^{3_1}$) represents the junction of two sheets: one associated with a semi-stable 3_1-cycle, and the other with an unstable 3_1-cycle. The flip curve ${}^{1}\Lambda_{3}^{3_1}$ (respectively ${}^{2}\Lambda_{3}^{3_1}$) is located on the sheets related to the 3_1-cycles. It consists of two segments that meet at the points C_i (for $i = 1, 2, 4$), each segment being the beginning of a sheet: One is associated with a semi-stable 3_1-cycle, and the other with an unstable 3_1-cycle.

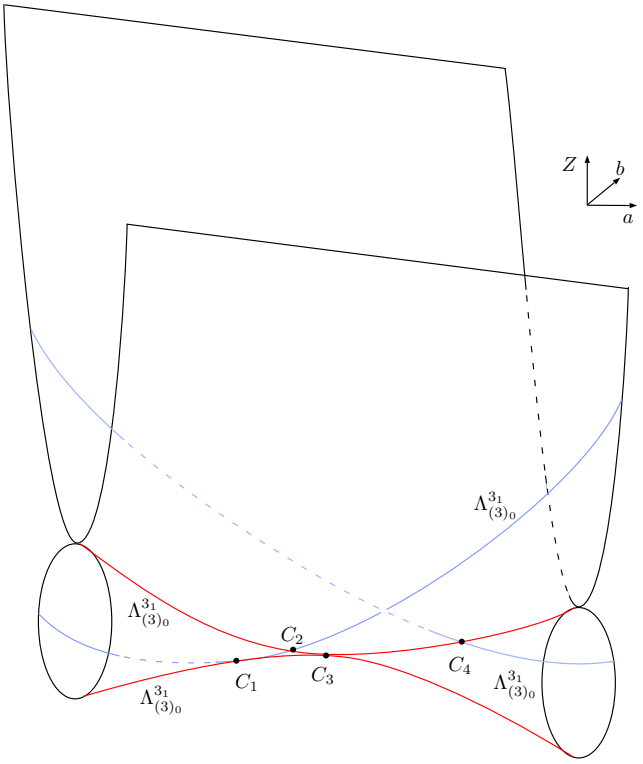

Figure 13. Foliation of parametric-plan of the 3-cycle 3_1.

Figure 14 displays the bifurcation diagram of the spatiotemporal quadratic map f in the (a, b) parameter plane for the $3_{3\_}$-cycle. The corresponding foliation is qualitatively depicted in Figure 15.

The fold curves ${}^{j}\Lambda^{3_{3-}}_{(3)_0}$ (for $j = 1, 2$), which represent the junction of two sheets, correspond to the emergence of two 3_{3-} cycles: one stable or semi-stable and the other unstable. In Figure 15, the orange and blue regions indicate the stability or semi-stability of the 3_{3-} cycles, while the white regions correspond to the instability of the 3_{3-} cycles. The curves ${}^{j}\Lambda^{3_{3-}}_{3}$ (for $j = 1, 2$) represent two distinct branches of the flip bifurcation curves associated with the 3_{3-} cycles and their corresponding fold curves.

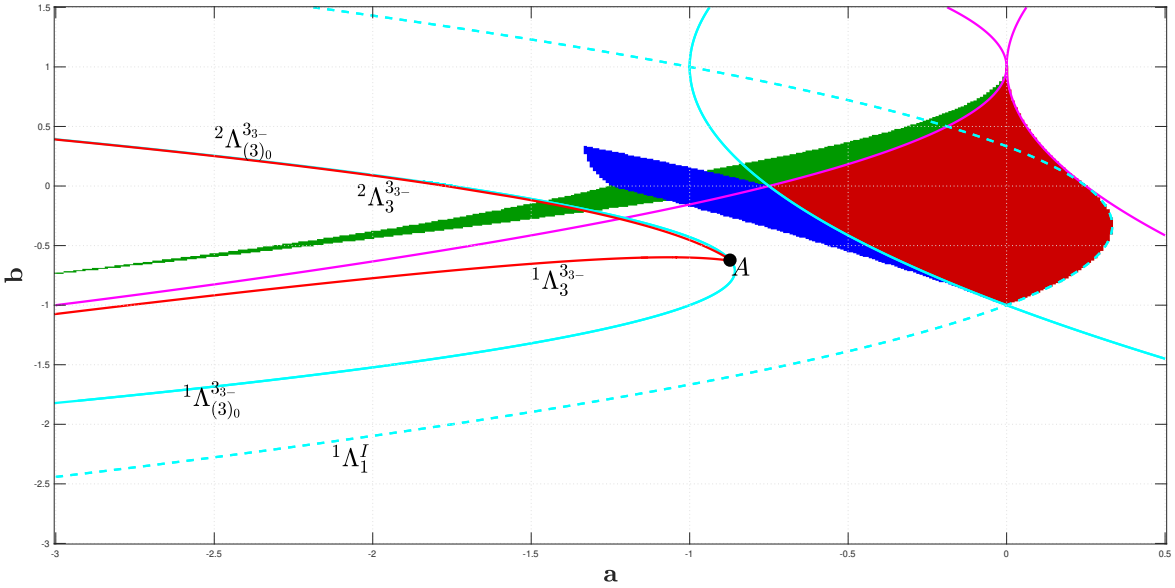

Figure 14. Bifurcation curves related to the 3-cycle 3_{3-}.

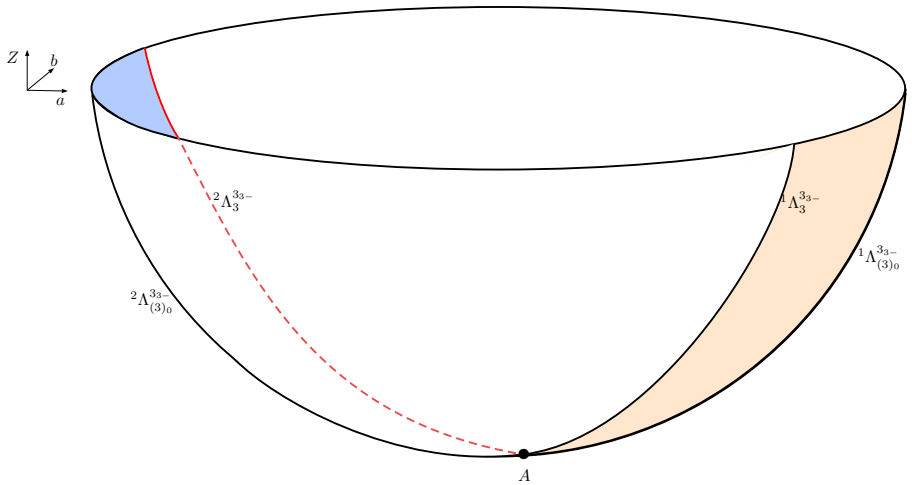

Figure 15. Foliation of parametric-plan for the 3_{3-}-cycle.

At the singular point A, the flip curves ${}^{j}\Lambda^{3_{3-}}_{3}$ (for $j = 1, 2$) are tangential to the corresponding fold curves ${}^{j}\Lambda^{3_{3-}}_{(3)_0}$. At this point, two of the three multipliers associated with A are $S_1 = -S_2 = \{1\}$.

Figure 16 shows the bifurcation curves of the spatiotemporal quadratic map f in the $(a,\ b)$ parameter plane for the 3_+ cycle. The corresponding foliation is qualitatively illustrated in Figure 17. In this figure, the flip bifurcation curves are denoted by ${}^{j}\Lambda_3^{3_{3+}}$, while the fold bifurcation curves are represented by ${}^{j}\Lambda_{(3)_0}^{3_{3+}}$, where $j = 1,\ 2,\ 3$. The fold curves $\Lambda_{(3)_0}^{3_{3+}} = {}^{1}\Lambda_{(3)_0}^{3_{3+}} \cup {}^{2}\Lambda_{(3)_0}^{3_{3+}} \cup {}^{3}\Lambda_{(3)_0}^{3_{3+}}$ correspond to the junction of two sheets, signifying the emergence of two 3_{3+} cycles one stable or semi-stable, and the other unstable. The flip curves $\Lambda_3^{3_{3+}} = {}^{1}\Lambda_3^{3_{3+}} \cup {}^{2}\Lambda_3^{3_{3+}} \cup {}^{3}\Lambda_3^{3_{3+}}$ are associated with their corresponding fold curves of the same index j.

At the singular points A_i (for $i = 1,\ 2$), the flip curves ${}^{j}\Lambda_3^{3_{3+}}$ (for $j = 1,\ 2$) are tangential to the fold curves ${}^{j}\Lambda_{(3)_0}^{3_{3+}}$, with two of the three multipliers at A_i (for $i = 1,\ 2$) being $S_1 = -S_2 = \{1\}$. Conversely, at the singular point A_3, the flip curves ${}^{1}\Lambda_3^{3_{3+}}$ and ${}^{2}\Lambda_3^{3_{3+}}$ intersect, resulting in $S_1 = S_2 = \{-1\}$.

The red and blue regions in Figure 16 represent the stability or semi-stability regions of the 3_{3+} cycles, while the white regions indicate the instability regions of these cycles.

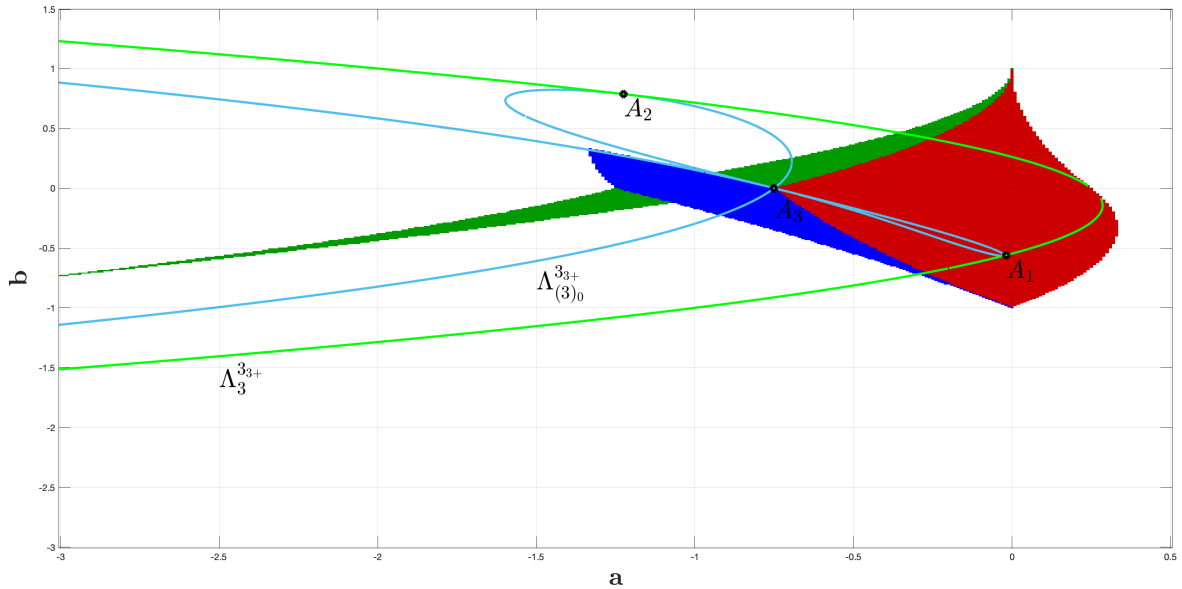

Figure 16. Bifurcation curves related to the 3_{3+}-cycle.

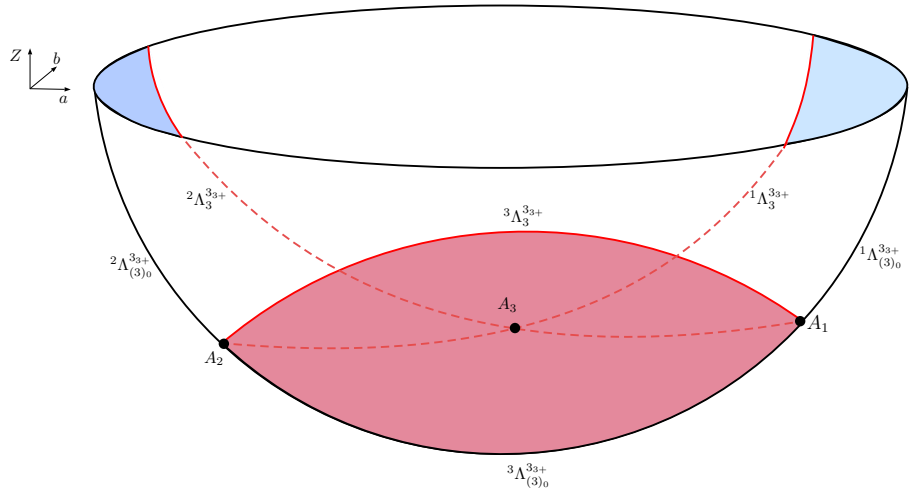

Figure 17. Foliation of parametric-plan for the 3-cycle 3_{3+}.

To complete the analysis of bifurcations for the spatiotemporal quadratic map f in the (a, b) parameter plane, we now present the bifurcation structure of the SD cycle, denoted as 3_2. This study focuses on the case of the first box, as discussed in [28]. Figure 18 illustrates the bifurcation curves of the 3_2 cycle, while the foliation is qualitatively depicted in Figure 19. In Figure 18, the flip bifurcation curves are denoted by $\Lambda_3^{3_2}$ and $\overline{\Lambda}_3^{3_2}$, while the fold bifurcation curves are labeled as ${}^{j,k}\Lambda_{(3)_0}^{3_2}$, where $j = 1, 2, 3$ differentiates the curves of the same cycle and $k = a$ or $k = b$ distinguishes the different branches of these fold bifurcation curves. The fold curves $\Lambda_{(3)_0}^{3_2} = {}^{1,a}\Lambda_{(3)_0}^{3_2} \cup {}^{1,b}\Lambda_{(3)_0}^{3_2} \cup {}^{2}\Lambda_{(3)_0}^{3_2}$ (and ${}^{3}\Lambda_{(3)_0}^{3_2}$) correspond to the junction of two sheets, indicating the emergence of four 3_2 cycles, two stable or semi-stable and two unstable. The branches ${}^{1,a}\Lambda_{(3)_0}^{3_2}$ and ${}^{1,b}\Lambda_{(3)_0}^{3_2}$ merge, each giving rise to two 3_2 cycles, one stable or semi-stable and the other unstable.

To understand the appearance and disappearance of the 3_2 cycle and their stabilities, consider the cross-section shown in Figure 19-(ii), where the parameter a is fixed at -1 and b increases from -3 to 0.5. In Figure 19-(i), the points K_i $(i = 1, 2, 3, 4)$ indicate cycles related to fold bifurcations, where the appearance or disappearance of cycles occurs. As b increases, 3_2 cycles appear through fold bifurcations, leading to a total of four cycles (semi-stable or unstable). Before the point K_1 $(K_1 \in {}^{2}\Lambda_{(3)_0}^{3_2})$, there is no SD cycle (considering the first box, see [28]). After crossing K_1, two SD cycles emerge, one semi-stable and one unstable. As b continues to increase, we reach the point K_2 $(K_2 \in {}^{3}\Lambda_{(3)_0}^{3_2})$, where two additional SD cycles appear, one unstable and one semi-stable. At points K_3 $(K_3 \in {}^{1,a}\Lambda_{(3)_0}^{3_2})$ and K_4 $(K_4 \in {}^{1,b}\Lambda_{(3)_0}^{3_2})$, the four SD cycles disappear, indicating the end of the 3_2 cycles beyond the fold bifurcation curve.

The flip bifurcation curves associated with the fold curves are $\Lambda_3^{3_2} = {}^{1,a}\Lambda_3^{3_2} \cup {}^{2}\Lambda_3^{3_2}$ and $\overline{\Lambda}_3^{3_2} = {}^{1,b}\Lambda_3^{3_2} \cup {}^{3}\Lambda_3^{3_2}$. The flip curve ${}^{1,a}\Lambda_3^{3_2}$ is associated with the fold curve ${}^{1,a}\Lambda_{(3)_0}^{3_2}$, with the stability region (red region in Figure 18) bounded by these two curves. Similarly, the curve ${}^{2}\Lambda_3^{3_2}$ is associated with the fold curve ${}^{2}\Lambda_{(3)_0}^{3_2}$, with the stability region (blue region in Figure 18) bounded by these two curves. At the singular point C, the flip curve $\Lambda_3^{3_2}$ is tangential to the fold curve $\Lambda_{(3)_0}^{3_2}$, with two multipliers corresponding to C given by $S_1 = -S_2 = \{1\}$.

Similarly, the flip bifurcation curve $\overline{\Lambda}_3^{3_2} = {}^{1,b}\Lambda_3^{3_2} \cup {}^{3}\Lambda_3^{3_2}$ consists of the branches ${}^{1,b}\Lambda_3^{3_2}$ and ${}^{3}\Lambda_3^{3_2}$. The flip curve ${}^{1,b}\Lambda_3^{3_2}$ is associated with the fold curve ${}^{3}\Lambda_{(3)_0}^{3_2}$, and the flip curve ${}^{3}\Lambda_3^{3_2}$ is associated with

the fold curve ${}^{1,b}\Lambda^{3_2}_{(3)_0}$. The stability regions (orange region) are bounded by these four curves.

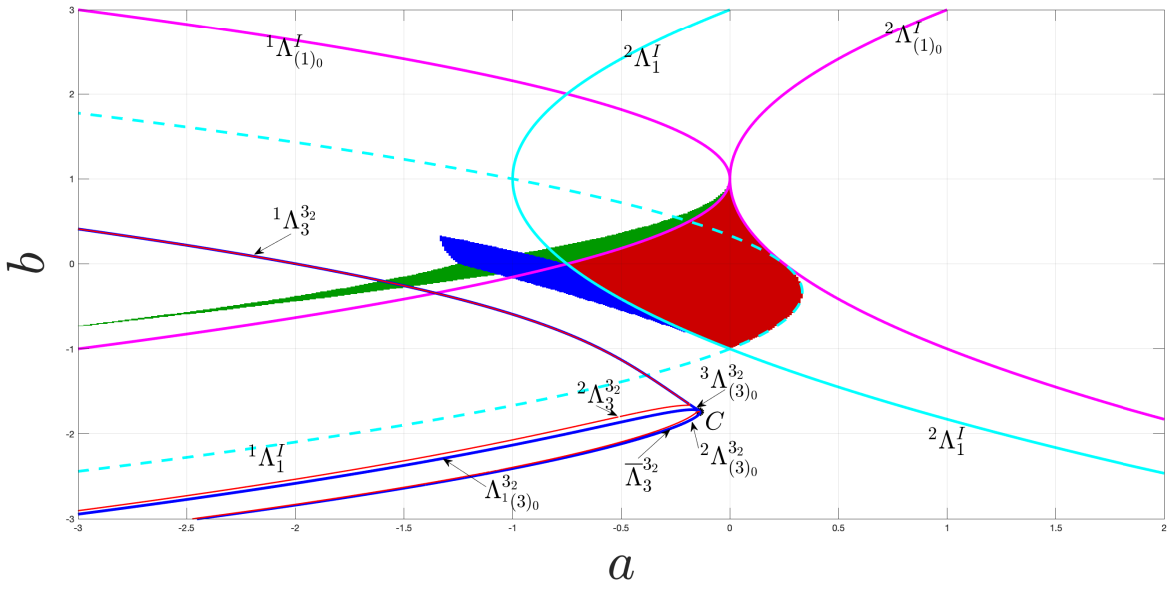

Figure 18. Bifurcation curves related to the 3-cycle 3_2.

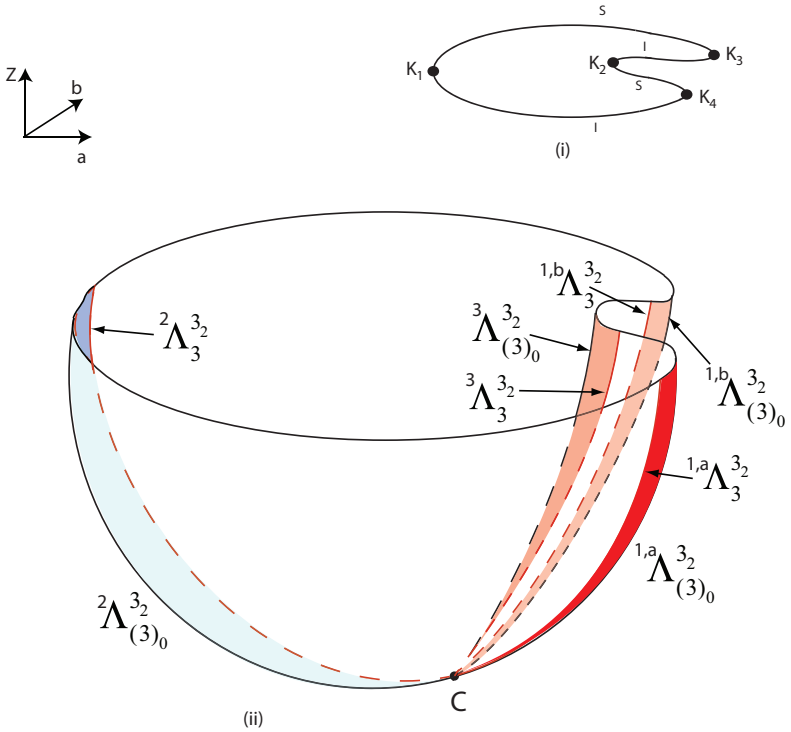

Figure 19. Foliation of parametric-plan for the 3-cycle 3_2.

4. Conclusions

This study highlights the intricate dynamics of 2D spatiotemporal discrete systems, particularly focusing on the stability and bifurcations of periodic solutions such as 3-cycles. The analysis of various types of 3-periodic points, categorized into four types (horizontal (H), super diagonal (SD), diagonal (D), and anti-diagonal (AD)), provides a comprehensive understanding of their stability conditions, which are determined by the spectral properties of the Jacobian matrix.

The study emphasizes the importance of bifurcation curves in illustrating how changes in parameters a and b can lead to qualitative shifts in system behavior, including the emergence of chaos or the stabilization of cycles. The findings reveal the intricate interplay between stability and bifurcations, particularly through the examination of a spatiotemporal quadratic map, which serves as a significant model for understanding nonlinear dynamics.

Key insights include the identification of stable and unstable 3-cycles, the transition from stability to chaos as parameters vary, and the detailed mathematical framework that supports the analysis of these cycles. The paper also highlights the role of numerical results, such as bifurcation diagrams, in visualizing the stability regions of fixed points and periodic orbits.

In conclusion, this study contributes to the understanding of the dynamics of 2D spatiotemporal discrete systems through bifurcation and periodicity analysis, and also suggests future research directions. These include potential applications to real-world phenomena such as pattern formation and epidemic propagation, thus providing valuable insights to the field of dynamical systems.

Author contributions

All authors contributed equally to the development of the research, analysis, and writing of the manuscript. All authors have read and agreed to the published version of the manuscript.

Use of Generative-AI tools declaration

The authors confirm that they utilized Generative-AI tools exclusively for formatting purposes during the final proofreading stage of their paper. No AI-generated content was used to influence the scientific analysis, results, or conclusions presented in the study.

Conflict of interest

The authors declare that there are no conflicts of interest regarding the publication of this paper.

References

1. K. R. Crounse, L. O. Chua, Methods for image processing and pattern formation in cellular neural networks: A tutorial, *IEEE Trans. Circuits Syst. I*, **42** (1995), 583–601. https://doi.org/10.1109/81.473566
2. Z. Lv, F. Sun, C. Cai, A new spatiotemporal chaotic system based on two-dimensional discrete system, *Nonlinear Dyn.*, **109** (2022), 3133–3144. https://doi.org/10.1007/s11071-022-07585-2

3. V. I. Nekorkin, M. G. Velarde, *Synergetic phenomena in active lattices: patterns, waves, solitons, chaos*, Springer, 2002. https://doi.org/10.1007/978-3-642-56053-8
4. Y. Song, X. Zou, Spatiotemporal dynamics in a diffusive ratio-dependent predator–prey model near a Hopf–Turing bifurcation point, *Comput. Math. Appl.*, **67** (2014), 1978–1997, 2014. https://doi.org/10.1016/j.camwa.2014.04.015
5. Y. Tao, W. Cui, Z. Zhang, Spatiotemporal chaos in multiple dynamically coupled map lattices and its application in a novel image encryption algorithm, *J. Inf. Secur. Appl.*, **55** (2020), 102650. https://doi.org/10.1016/j.jisa.2020.102650
6. C. Tian, On the pseudo-randomicity of discrete spatiotemporal systems, *Int. J. Bifurcat. Chaos*, **24** (2014), 1450013. https://doi.org/10.1142/s0218127414500138
7. C. Tian, Chaos in the sense of Devaney for two-dimensional time-varying generalized symbolic dynamical systems, *Int. J. Bifurcat. Chaos*, **27** (2017), 1750060. https://doi.org/10.1142/s0218127417500602
8. C. Tian, Hypercyclicity for a class of discrete spatiotemporal systems, *Int. J. Bifurcat. Chaos*, **27** (2017), 1750045. https://doi.org/10.1142/s0218127417500456
9. C. Tian, G. Chen, Stability and chaos in a class of 2-dimensional spatiotemporal discrete systems, *J. Math. Anal. Appl.*, **356** (2009), 800–815. https://doi.org/10.1016/j.jmaa.2009.03.046
10. R. Chen, F. Zhang, L. Teng, X. Wang, Cross-image encryption algorithm based on block recombination and spatiotemporal chaos system, *J. Opt.*, **52** (2023), 2109–2129. https://doi.org/10.1007/s12596-023-01104-1
11. E. Fornasini, A 2-D systems approach to river pollution modelling, *Multidimens. Syst. Signal Process.*, **2** (1991), 233–265. https://doi.org/10.1007/bf01952235
12. E. Fornasini, G. Marchesini, Doubly-indexed dynamical systems: State-space models and structural properties. *Math. Syst. Theory*, **12** (1978), 59–72. https://doi.org/10.1007/bf01776566
13. J. Fritz, *Partial Differential Equations*, volume 1. Springer Science & Business Media, 1991. https://doi.org/10.1007/978-1-4419-1096-7_5
14. S. Liu, F. Sun, Spatial chaos-based image encryption design, *Sci. China Ser. G*, **52** (2009), 177–183. https://doi.org/10.1007/s11433-009-0032-2
15. Y. Ma, Y. Tian, L. Zhang, P. Zuo, Two-dimensional hyperchaotic effect coupled mapping lattice and its application in dynamic s-box generation, *Nonlinear Dyn.*, **112** (2024), 17445–17476. https://doi.org/10.1007/s11071-024-09907-y
16. R. Roesser, A discrete state-space model for linear image processing, *IEEE Trans. Autom. Control*, **20** (1975), 1–10. https://doi.org/10.1109/tac.1975.1100844
17. F. Sun, S. Liu, Z. Li, Z. Lü, A novel image encryption scheme based on spatial chaos map, *Chaos Soliton. Fract.*, **38** (2008), 631–640. https://doi.org/10.1016/j.chaos.2008.01.028
18. F. H. Willeboordse, The spatial logistic map as a simple prototype for spatiotemporal chaos, *Chaos*, **13** (2003), 533–540. https://doi.org/10.1063/1.1568692
19. C. Yuan, S. Liu, Exact regions of oscillation for a mixed 2D discrete convection system, *J. Differ. Equ. Appl.*, **21** (2015), 37–52. https://doi.org/10.1080/10236198.2014.979167
20. K. Sarkar, S. Khajanchi, Spatiotemporal dynamics of a predator-prey system with fear effect, *J. Franklin Inst.*, **360** (2023), 7380–7414. https://doi.org/10.1016/j.jfranklin.2023.05.034

21. E. M. Izhikevich, *Dynamical systems in neuroscience*, MIT Press, 2007. https://doi.org/10.7551/mitpress/2526.001.0001
22. L. Randriamihamison, A. K. Taha, About the singularities and bifurcations of double indices recursion sequences, *Nonlinear Dyn.*, **66** (2011), 795–808. https://doi.org/10.1007/s11071-011-9952-2
23. M. L. Sahari, A. K. Taha, L. Randriamihamison, Stability and bifurcations in 2D spatiotemporal discrete systems, *Int. J. Bifurcat. Chaos*, **28** (2018), 1830026. https://doi.org/10.1142/s0218127418300264
24. M. L. Sahari, A. K. Taha, L. Randriamihamison, Bifurcations in 2D spatiotemporal maps, *Int. J. Bifurcat. Chaos*, **31** (2021), 2150091. https://doi.org/10.1142/s0218127421500917
25. M. L. Sahari, A. K. Taha, L. Randriamihamison, A note on the spectrum of diagonal perturbation of weighted shift operator, *Le Matematiche*, **74** (2019), 35–47, 2019. http://dx.doi.org/10.48550/arXiv.1609.05203
26. P. R. Halmos, *Introduction to Hilbert space and the theory of spectral multiplicity*, Courier Dover Publications, 2017. https://doi.org/10.2307/3608269
27. Y. A. Kuznetsov, I. A. Kuznetsov, Y. Kuznetsov, *Elements of applied bifurcation theory*, volume 112. Springer, 1998. https://doi.org/10.1007/978-1-4757-2421-9
28. I. Gumowski, C. Mira, *Dynamique chaotique: Transformations ponctuelles, transition, ordre-désordre*. Cepadues, 1980. https://doi.org/10.1002/zamm.19810611023
29. C. Mira, Chaos and fractal properties induced by noninvertibility of models in the form of maps, *Chaos Soliton. Fract.*, **11** (2000), 251–262. https://doi.org/10.1016/s0960-0779(98)00291-4
30. A. L. Shields, Weighted shift operators and analytic function theory, *Math. Surv.*, **13** (1974), 49–128. https://doi.org/10.1090/surv/013/02
31. P. R. Halmos, *A Hilbert space problem book*, volume 19, Springer Science & Business Media, 2012. https://doi.org/10.1007/978-1-4684-9330-6
32. W. B. Gordon, Period three trajectories of the logistic map, *Math. Mag.*, **69** (1996), 118–120. https://doi.org/10.1080/0025570x.1996.11996403
33. M. H. Lee, Three-cycle problem in the logistic map and Sharkovskii's theorem, *Acta Phys. Pol. B*, **42** (2011). https://doi.org/10.5506/APhysPolB.42.1071
34. M. H. Lee, Solving for the fixed points of 3-cycle in the logistic map and toward realizing chaos by the theorems of Sharkovskii and Li-Yorke, *Commun. Theor. Phys.*, **62** (2014), 485. https://doi.org/10.1088/0253-6102/62/4/06
35. P. Saha, S. H. Strogatz, The birth of period three, *Math. Mag.*, **68** (1995), 42–47. https://doi.org/10.1080/0025570x.1995.11996273
36. J. C. Cathala, H. Kawakami, C. Mira, Singular points with two multipliers, s1=- s2= 1, in the bifurcation curves of maps, *Int. J. Bifurcat. Chaos*, **2** (1992), 1001–1004. https://doi.org/10.1142/s0218127492000616

AIMS Press